(12)

AD

LEVEL II

(18) (19)

AMMRC TR 78-23

(6) MACHINE CASTING OF FERROUS ALLOYS,

(11) MAY 1978 (12) 69 p.

(10) R. MEHRABIAN, D. G. BACKMAN, G. J. ABBASCHIAN, C. Y. CHEN, S. HONG, S. D. E. RAMATI, and Y. V. MURTY
Department of Metallurgy and Mining Engineering
Department of Mechanical and Industrial Engineering
University of Illinois at Urbana-Champaign
Urbana, Illinois 61801

(9) Final Report. 1 Oct 75— 31 Dec 77,

(15) Contract Number DAAG46-76-C-0023,

Sponsored by: Defense Advanced Research Projects Agency, ARPA Order No. 2267
Program Code No. 6Y10
Effective Date of Contract: October 1, 1975
Contract Expiration Date: December 31, 1977
Amount of Contract: $199,930
Contract Period Covered by Report: October 1, 1975-December 31, 1977

Approved for public release; distribution unlimited.

Prepared for

ARMY MATERIALS AND MECHANICS RESEARCH CENTER
Watertown, Massachusetts 02172

The findings in this report are not to be construed as an official Department of the Army position, unless so designated by other authorized documents.

Mention of any trade names or manufacturers in this report shall not be construed as advertising nor as an official indorsement or approval of such products or companies by the United States Government.

DISPOSITION INSTRUCTIONS

Destroy this report when it is no longer needed.
Do not return it to the originator.

UNCLASSIFIED

SECURITY CLASSIFICATION OF THIS PAGE (When Data Entered)

REPORT DOCUMENTATION PAGE	READ INSTRUCTIONS BEFORE COMPLETING FORM
1. REPORT NUMBER: AMMRC TR 78-23 ✓	2. GOVT ACCESSION NO. / 3. RECIPIENT'S CATALOG NUMBER
4. TITLE (and Subtitle): MACHINE CASTING OF FERROUS ALLOYS	5. TYPE OF REPORT & PERIOD COVERED: Final Report
	6. PERFORMING ORG. REPORT NUMBER
7. AUTHOR(s): R. Mehrabian, D. G. Backman, G. J. Abbaschian, C. Y. Chen, S. Hong, S. D. E. Ramati, and Y. V. Murty	8. CONTRACT OR GRANT NUMBER(s): DAAG46-76-C-0023 ✓
9. PERFORMING ORGANIZATION NAME AND ADDRESS: Department of Metallurgy and Mining Engineering, Department of Mechanical and Industrial Engr. ✓, University of Illinois, Urbana, IL 61801	10. PROGRAM ELEMENT, PROJECT, TASK AREA & WORK UNIT NUMBERS: D/A Project: 2267, AMCMS Code: 6Y10, Agency Accession:
11. CONTROLLING OFFICE NAME AND ADDRESS: Army Materials and Mechanics Research Center, Watertown, Massachusetts 02172	12. REPORT DATE: May 1978
	13. NUMBER OF PAGES
14. MONITORING AGENCY NAME & ADDRESS (if different from Controlling Office): Army Materials and Mechanics Research Center, Watertown, Massachusetts 02172	15. SECURITY CLASS. (of this report): Unclassified
	15a. DECLASSIFICATION/DOWNGRADING SCHEDULE

16. DISTRIBUTION STATEMENT (of this Report)

Approved for public release; distribution unlimited.

17. DISTRIBUTION STATEMENT (of the abstract entered in Block 20, if different from Report)

18. SUPPLEMENTARY NOTES

19. KEY WORDS (Continue on reverse side if necessary and identify by block number)

Die casting
Solidification
Ferrous Alloys

20. ABSTRACT (Continue on reverse side if necessary and identify by block number)

This is the fourth and final report describing research conducted at the University of Illinois at Urbana-Champaign as part of a joint University-Industry research program on machine casting of high temperature alloys. It covers the period of 30 months, 1 October 1975 to 31 December, 1977. The work at the University of Illinois was initiated at a time when the overall program had already been in effect for 33 months. The initial aim of the overall program was to plan and test new and innovative processes and devel- → over ✓

DD FORM 1 JAN 72 1473 EDITION OF 1 NOV 65 IS OBSOLETE

UNCLASSIFIED

SECURITY CLASSIFICATION OF THIS PAGE (When Data Entered)

Block No. 20

ABSTRACT

op a machine casting system for ferrous alloys that would produce good quality parts economically and at high speed.

Emphasis of the work at the University of Illinois was on processes and casting systems which employ a partially solid alloy as charge material. The program was especially designed to establish the processing conditions necessary to produce porosity-free parts and to evaluate the Rheocasting and Thixocasting processes from both a technical and economical point of view.

During the first eighteen months, work was performed and reported on the following subjects:

1. A variety of casting systems were designed, constructed, and operated; these include the following:
   (a) A transparent model continuous slurry producer,
   (b) A low-temperature alloy continuous slurry producer and a direct chill assembly that permits production of Rheocast ingots semi-continuously,
   (c) A high-temperature alloy continuous slurry producer, and
   (d) A laboratory casting machine which permits direct observation and photography of mold filling.

2. The important relationships between process variables and the structure of continuously produced partially solidified slurries were established.

3. The relationships between gating systems, process variables, and mold filling characteristics of different viscosity materials and low temperature alloy slurries were studied in the transparent casting machine.

4. The effect of cast (Rheocast) structure on microsegregation, solution heat treatment response, and mechanical properties of high temperature alloys were studied.

5. A cost analysis model was developed to permit economic evaluation of the new machine casting process.

In the last year of the contract, work was carried out on two of the topics listed above (items 4 and 5).

Analytical and computer models were developed for solutionizing of Rheocast and conventional cast (dendritic) alloys. The predictions were compared with experiment on a model alloy system, 2024 aluminum base alloy. Recent results of die life studies obtained from M.I.T. were incorporated in the cost analysis model developed earlier and a cost per piece for a previously investment cast part was calculated for manufacture via the new machine casting process.

This final report summarizes earlier results reported in the first eighteen months of the program and covers the details of the last 12 months

FOREWORD

This research was supported by the Advanced Research Projects Agency of the Department of Defense and was monitored by the Army Materials and Mechanics Research Center under Contract No. DAAG46-76-C-0023. Technical monitor of this Contract was Mr. F. C. Quigley.

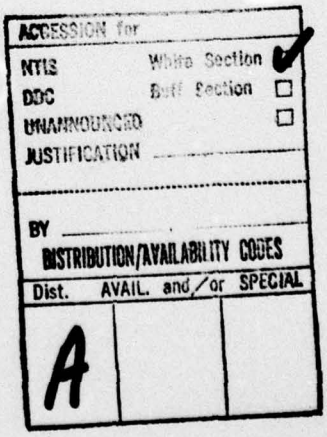

TABLE OF CONTENTS

I. INTRODUCTION

This is the fourth and final report describing research conducted at the University of Illinois at Urbana-Champaign as part of a joint University-Industry research program on machine casting of high temperature alloys. It covers the period of 30 months, 1 October 1975 to 31 December, 1977. The work at the University of Illinois was initiated at a time when the overall program had already been in effect for 33 months. The initial aim of the overall program was to plan and test new and innovative processes and develop a machine casting system for ferrous alloys that would produce good quality parts economically and at high speed.

Emphasis of the work at the University of Illinois was on processes and casting systems which employ a partially solid alloy as charge material. The program was especially designed to establish the processing conditions necessary to produce porosity-free parts and to evaluate the Rheocasting and Thixocasting processes from both a technical and economical point of view.

The specific objectives of the investigations included the following:

(1) development of the important relationships between process variables in the Rheocasting and Thixocasting systems and the quality of the machine cast parts made from the partially solidified slurries,

(2) determination of the effect of cast (Rheocast) structure on microsegregation, solution heat treatment response and mechanical properties of ferrous alloys and superalloys, and

(3) development of an economic model based on die life studies carried out at M.I.T. (one of the participants in the program) to project cost per part for the new machine casting process.

During the first eighteen months, work was performed and reported [1, 2, 3] on the following subjects:

1. A variety of casting systems were designed, constructed, and operated; these include the following:
   (a) A transparent model continuous slurry producer,
   (b) A low-temperature alloy continuous slurry producer and a direct chill assembly that permits production of Rheocast ingots semi-continuously,
   (c) A high-temperature alloy continuous slurry producer, and
   (d) A laboratory casting machine which permits direct observation and photography of mold filling.
2. The important relationships between process variables and the structure of continuously produced partially solidified slurries were established.
3. The relationships between gating systems, process variables, and mold filling characteristics of different viscosity materials and low temperature alloy slurries were studied in the transparent casting machine.
4. The effect of cast (Rheocast) structure on microsegregation, solution heat treatment response, and mechanical properties of high temperature alloys were studied.
5. A cost analysis model was developed to permit economic evaluation of the new machine casting process.

In the last year of the contract, work was carried out on two of the topics listed above (items 4 and 5).

Analytical and computer models were developed for solutionizing of Rheocast and conventional cast (dendritic) alloys. The predictions were compared with experiment on a model alloy system, 2024 aluminum base alloy. Recent results of die life studies obtained from M.I.T. were incorporated in the cost analysis model developed earlier and a cost per piece for a previously investment cast part was calculated for manufacture via the new machine casting process.

This final report summarizes earlier results reported in the first eighteen months of the program [1, 2, 3] and covers the details of the investigation in the last twelve months.

II. THE EFFECT OF PROCESS VARIABLES ON THE STRUCTURE OF A PARTIALLY SOLIDIFIED SLURRY

The general aim of this portion of the investigation was to establish the effect of process variables on the structure of slurries of alloys produced continuously and to compare and contrast these structures with conventional dendritic structures solidified under identical cooling rates. The need for such a study was based on the recognition that the structure of a partially solid slurry effects both its rheological behavior during the shape forming operation and the subsequent properties of the parts produced. Hence, control of this structure is essential if this new technology is to be successfully applied to casting or forming of high quality, heat treatable parts with acceptable properties.

Three continuous slurry production apparatuses were designed, built and operated with a variety of low temperature model systems and high temperature alloys. These included:

(a) a transparent model continuous slurry producer,

(b) a low temperature continuous slurry producer and a direct chill assembly that permits production of Rheocast ingots semi-continuously, and

(c) a high temperature continuous slurry producer.

The effect of machine design and the operating variables (e.g. power input, cooling capacity , flow rate, etc.) on the process variables during slurry production and the effect of the latter on the structure of Rheocast slurries were studied using the following model and alloy systems; NH_4Cl - H_2O, Sn-15% Pb, 2024 aluminum base alloy, 905 copper base alloy, 304 stainless steel, 440C stainless

steel and X-40 cobalt base alloy. In a corollary experimental program,relationships between primary and secondary dendrite arm spacings were determined for two of the alloys, Sn-15% Pb and X-40 cobalt base alloy. Results of work on the effect of average cooling rate on primary particle size in continuously produced slurries were then compared with the segregate spacings in the dendritically solidified specimens.

Detailed description of the apparatuses, and their operating procedures and our findings relating process variables to the structure of the slurries, and comparison of the latter with conventional dendritic structures have previously been reported [1, 2, 3]. Only a few figures, some representative microstructures and a summary of the most important findings are presented herein.

Figure 1 shows a schematic of the high temperature continuous slurry producer. Most recent modifications of the apparatus include protection of the melt in the top chamber and the exiting slurry from the lower chamber with an Argon - 4% Hydrogen gas atmosphere. The basic design of the transparent and the low temperature slurry producers are similar to Figure 1 except for appropriate substitution of crucible and rotor materials, heating and cooling systems.

Figure 2 shows representative microstructures of slurries of NH_4Cl-H_2O, Sn-15% Pb, 440C stainless steel and X-40 cobalt base superalloy. Note that the liquid was drained from the NH_4Cl-H_2O structure to reveal the spheroidal particles solidified during primary solidification. On the other hand, the Sn-15% Pb specimen was cooled about an order of magnitude faster than the other two alloys.

Important findings from this work include the following:

(a) Utilization a round rotor in the lower mixing chamber led

to formation of flow instabilities known as Taylor Rings. This phenomena was directly observed and photographed in the transparent system during production of NH_4Cl-H_2O slurries. These flow instabilities were eliminated when a rotor with a square cross-section in the lower chamber was used.

(b) The three important process variables affecting the structure and viscosity of continuously produced slurries are average shear and cooling rates and volume fraction solid.

(c) Average cooling rate has the most pronounced effect on the structure of a slurry. Increasing the average cooling rate makes the primary solid particles more uniform and smaller in size, Figures 3 and 4, but increases the relative amount of entrapped liquid in each particle - increases the effective volume fraction of solid in the slurry, hence increases it's viscosity.*

(d) Average shear rate affects particle size and uniformity of size similarly, though this effect is noted only at low cooling rates. In general, increasing average shear rate reduces the amount of entrapped liquid in the primary particles resulting in a corresponding decrease in viscosity.*

(e) As the volume fraction solid in a slurry increases, so does it's viscosity.*

(f) Primary dendrite arm spacings in conventional castings and primary particle size in continuously produced slurries are of the same order of magnitude if average cooling rates during solidification are identical, Figure 3 and 5.

The general trends established between shear and cooling rates and the structure and viscosity of a slurry are summarized in Table I.

* Relationships between structure and viscosity were deduced from earlier work carried out on a high temperature viscometer [4] and some indirect torque measurements (power consumption of the DC motor driving the rotor) in a continuous slurry apparatus.

III. TRANSPARENT MACHINE CASTING STUDIES

Transparent machine (die) casting studies were undertaken to analyze the relationship between process variables (kinematic viscosity of the charge material, gate velocity, gate and runner geometry and location) on fluid flow and air entrappment during die filling. Most of the results of this study were reported earlier [2] and were used by the Pratt and Whitney Aircraft Group* [5] in the design of the gating system for their simulated gas turbine shape Thixocasting. A short summary of the previous findings are combined with more recent experiments and are reported herein. An ongoing, long range, research effort at the University of Illinois on a Commercial horizontal die casting machine is aimed at verification of the phenomenological relationships established in this study.

The transparent casting machine was designed to simulate a commercial horizontal cold chamber die casting machine. One of the dies houses a flat ground quartz window through which flow of charge material through the gating system into the casting cavity can be directly observed and photographed with a high speed movie camera. A large number of experiments were conducted during which the machine casting parameters were varied. The process variables examined included:

(1) the kinematic viscosity of the charge material (.003 to 23.0 cm^2/sec, Stokes)

(2) the gate velocity (1 to 80 $m.sec^{-1} \sim 3.3$ to 262 $ft\ sec^{-1}$)

* The Pratt and Whitney Aircraft Group of the Commercial Products Division in East Hartford, Connecticut, was a member of this University-Industry research program.

(3) gate and runner geometry, and location

The effect of charge kinematic viscosity was studied by casting various organic fluids of known viscosity and Sn-Pb liquid and parrially solid slurries. Two casting cavity designs were investigated including a flat plate mold cavity ($\sim 0.1 \times 0.064 \times 0.318 \times 10^{-2}$ meters thick) and a simulated turbine blade casting cavity.

The results of experiments conducted with both the plate die and the turbine blade die showed that the kinematic viscosity of the charge and the ingate velocity influence the pattern of fluid flow emanating from the ingate. Qualitatively, it was found that at low velocity, high viscosity fluids fill the die cavity with a stable front as shown in Figure 6. However, as ingate velocity increases and charge viscosity decreases, the charge/air interface becomes unstable and atomization of charge occurs at the ingate. At intermediate values of velocity and viscosity, a transitional mode of filling is observed. These die filling patterns are shown in Figure 6.

By representing the mode of die filling observed during each experiment on a plot of Reynolds number, R_E, versus either the Z number or the Weber number, the quantitative relationship between process variables and flow regime was established. One of the plots determined from experiments conducted with various fluids, in both of the casting cavity designs, and several runner geometries is shown in Figure 7. On this plot, Regions I, II, and III represent the range of parameters during which solid front fill, transitional fill, and atomized die fill are achieved, respectively. These results confirm the qualitative results described above. For example, at a constant value of $Z = 1$, we find that solid front fill is observed when

R_E < 50 and atomized fill is obtained when R_E > 300. At intermediate values of Reynolds number transitional die filling cocurs.

The results of the experiments conducted show that the mode of die filling and the amount of gas entrapped during filling are controlled by the physical properties of the charge material and the geometry and location of the ingates. Specifically, reduced porosity, turbulence, and vorticity were observed when the cavity filled with a solid front. This condition of filling was established at low Reynolds numbers and hence with a low ingate velocity and with charge material having a high kinematic viscosity.

As reported in the previous section, the apparent viscosity (or apparent kinematic viscosity) of partially solidified slurries of metal alloys increases with increasing volume fraction of solid. Therefore, it is anticipated that as the volume fraction of solid in the charge material increases solid front fill can be achieved at relatively high gate velocities. A minimum gate velocity exists below which the charge would solidify before the die cavity is completely full. Experiments with partially solid slurries of Sn-15%Pb alloy have verified the above.

IV. SEGREGATION, SOLUTION HEAT TREATMENT AND MECHANICAL PROPERTIES OF RHEOCAST ALLOYS

A comprehensive study was undertaken in this program to determine the effect of cast (Rheocast) structure on microsegregation, mechanical properties and especially the solution heat treatment response of several alloys (2024 aluminum base alloy, 905 copper base alloy, 304 stainless steel, 440C stainless steel and X-40 cobalt base alloy). Most of the results of microsegregation and properties of the high temperature alloys were reported earlier [3]. Only the important findings from this work will be reviewed here. Results from this earlier work indicated that due to the significantly altered metallurgical structure there may be some differences between the solution heat treatment response of Rheocast ingots and conventionally solidified dendritic ingots. It was thus deemed desireable to carry out a detailed theoretical and experimental study on solution heat treatment response of a model system. This was done during the last twelve months of the contract with commercial 2024 aluminum alloy as the model system.

Results of this study will be presented in detail in this section.

A. Summary of Investigations on High Temperature Alloys

The alloys studied were 905 copper base alloy, 304 stainless steel, 440C stainless steel and X-40 cobalt base alloy. Typical Rheocast (water quenched) structures of two of the alloys are shown in Figure 2. Electron probe microanalysis of the water quenched slurries consistently showed relatively flat elemental composition profiles of alloying elements in the primary solid particles with

abrupt changes at their boundaries [1,3]. These segregation profiles differed from conventional dendritic microsegregation where a minimum or maximum concentration was usually observed at the center of dendrite arms. These differences can be ascribed to the faster solute diffusion in the spherical primary solid particles of the Rheocast slurries. The same effect was noted during solution heat treatment of Rheocast versus dendritic structures as described in the next section.

All the solution heat treatment and mechanical property measurements were carried out on static ingots cast into insulated molds ($\sim$ 0.032m in diameter by $\sim$ 0.18m high) using the high temperature continuous slurry producer. Due to the slower cooling rates, the primary solid particles coarsened during final solidification resulting in equiaxed structures, Figure 8.

Metallographic, electron probe microanalysis, microhardness and the measure mechanical properties indicated significant solute redistribution, dissolution and reprecipitation of second phases during solution heat treatment and subsequent aging of the stainless steels and the cobalt base alloy. For example, results from compression tests of as-Rheocast and solutionized 440C stainless steel are shown in Figure 9. Improvement in the yield strength of the as-Rheocast alloy with solution heat treatment is a direct consequence of transformation of the grain boundary M_7C_3 carbides to $M_{23}C_6$ carbides. This conversion is accompanied by the diffusion of carbon and homogeneous redistribution of the latter carbides within the equiaxed grains of the alloy [6]. Similarly, Figure 10 shows that during heat treatment of Rheocast X-40 cobalt base alloy; (a) some of the primary carbide phase in the interparticle boundaries

and reprecipitates as $M_{23}C_6$ type of carbides during very slow cooling from the solutionizing temperature, and (b) increasing the solution heat treatment temperature results in increased carbide dissolution and reprecipitation, as well as spherodization of the remaining interparticle carbides. Microhardness measurements carried out across the primary solid particles of the as-Rheocast and solutionized specimens shown in Figure 11 confirm these observations.

Room temperature mechanical properties and the compressive yield strength versus temperature of the as-Rheocast and dendritic X-40 cobalt base alloy are shown in Table II and Figure 12, respectively. The lower ductility and ultimate strength of the Rheocast ingots was due to poor feeding, microporosity formation, in these ingots during final solidification. On the other hand, the stress rupture properties were equivalent after closure of the microporosity by hot isostatic pressing. The changes in yield strength with solution heat treatment in Figure 12 can be attributed to redistribution of primary carbides by coarsening and changes in their chemistry.

B. Solution Heat Treatment Models: Comparison With Experiments

1. Background

This investigation was aimed towards the experimental measurement and the theoretical determination of solution kinetics during the heat treatment of both Rheocast and conventionally solidified 2024 aluminum base alloy.* The specific motivation for the investigation was two fold; (a) to determine whether the differences in

* Nominal composition of 2024 aluminum base alloy is Al-4.5% Cu-1.5% Mg-0.6% Mn-0.25% Fe-0.10% Si

microstructure and solidification segregation profiles between the two processing techniques cause a significant alteration in solution kinetics, and (b) to provide a predictive model which will enable the establishment of practical solutionizing prodedures for Rheocast metals.

Numerous investigators have studied the solution treatment of cast dendritic metals. These investigations have employed quantitative metallographic techniques to measure the amount of eutectic present as a function of both heat treatment temperature and time. Correspondingly, both mathematical solutions and computer simulation have been adopted to analyze the behavior of many alloys during solution treatment. Singh and Flemings [7] assumed a plate dendrite model with an initial sinusoidal composition profile within the primary phase. Using the further assumption that solution kinetics is not affected by interface motion, they derived the following equation:

$$\frac{g + a}{g_o + a} = \exp\left[- \frac{D_s t}{\ell_o^2} \cdot \frac{\pi^2}{4} \right] \qquad (1)$$

Where:

g = volume fraction of the second phase at time t

g_o = volume fraction of the second phase at t=0

D_s = diffusion coefficient at the solution temperature

ℓ_o = one half the dendrite arm spacing

t = time of solution treatment

$$a = \frac{C_m - C_o}{C_\beta}$$

C_m = maximum soluability at the solution temperature, gm per cu. cm

C_o = initial composition, gm per cu. cm

C_β = composition of the second phase, gm per cu. cm

Using this model they obtained good agreement with experimentally determined solution kinetics for Al-Cu alloys.

Singh et al[8] also developed an explicit computer simulation technique to describe the solutionizing of materials containing plate like dendrites. This model included both diffusion within the primary phase and motion of the single phase interface determined by a mass balance. Their results agreed well with experiment at short times, however, at long times the predicted velocity of the interface was higher than the experimentally measured velocity. They attributed this discrepancy to the fact that the actual dendrite morphology is complex and that second phase present between primary dendrites must diffuse over longer distances than the material between secondary dendrite arms. As a consequence they concluded that second phase within the primary dendrite dissolves rapidly whereas solutionization of second phase on the periphery of the primary dendrite requires a long time.

Other investigators including Tanzilli and Heckel[9] and Teleshov and Zolortorevisky[10] have developed predictive models which can be applied to the determination of solutionizing times. Assuming a plate dendrite morphology, Teleshov and Zolotorevsky[10] found that the time for complete solutionization is given by the following equation:

$$t_c = \frac{g_o\,[C_\beta - C_m]}{[(C_m - C_o) + \frac{g_o}{2}\,(C_\beta + C_m)]}\,(\frac{\ell_o^2}{D_s}) \qquad (2)$$

Tanzilli and Heckel[9] modelled the solution kinetics of precipitates. The initial condition used in their numerical analy-

sis was that both the primary and second phase regions have a uniform composition. However, the effect of interface motion upon solution kinetics was considered in the analysis. Singh, et al [8] compared the results of this analysis with their theoretical and experimental findings. They found that the analysis of Tanzilli and Heckel [9] produces faster solutionization than observed particularly at short times.

In the following sections both analytical and computer simulation models of solutionization of conventional cast and Rheocast 2024 aluminum base alloy are presented and compared to with those described above, and experimental findings of this investigation.

2. Experimental Procedure

Commercially pure 2024 aluminum base alloy was used to produce two ingots, one with a Rheocast structure and the second with a dendritic structure. The dendritic ingot was produced by pouring the molten alloy into a cylindrical graphite mold heated to $\sim$ 200°C. The preheating was provided to slow the rate of solidification so that the local solidification time equalled that obtained in the Rheocast ingot. The Rheocast ingot was produced using the high temperature slurry producer. The semi-solid aluminum alloy was discharged into a stainless steel ingot tube internally insulated with fiber frax paper. The insulation was necessary for the production of a filled and sound ingot.

After solidification each ingot was removed from the mold and quenched into water to minimize post solidification heat treatment. Subsequently, each ingot was cut into sections and the pieces were heat treated in a recirculating air furnace.

Heat treatment was carried out at 515°C for the following times: 0.5, 1, 3, 10, and 50 hrs. Two specimens from each of the two ingots were used in every heat treatment. After the heat treatment, the samples were quenched in water to room temperature and mounted for metallographic analysis. The polished and etched samples were quantitatively analyzed using a point counting technique. A 9 x 5 grid was utilized by repetitive random application yielding a total grid count of 1200 per specimen. The samples were analyzed at 200X giving volume fraction of second phase to an accuracy of ± 10% of the measured amount.

3. Solution Models

A computer program was developed to simulate the diffusive flow of solute during solidification and solutionizing heat treatment of the aluminum alloy. The model employs a plate-like dendrite geometry for the conventionally cast alloy and a spherical growth morphology for the partially solid (Rheocast) alloy. The simulation technique employs an explicit finite difference analysis to incorporate solute diffusion during processing. In order to facilitate solution, a number of simplifying assumptions were adopted:

(a) During solidification, the position of the liquid-solid interface is a linear function of time.

(b) There is local equilibrium at the liquid-solid interface and the ratio of compositions in the solid and liquid phases can be described by a constant partition coefficient, k.

(c) There is complete mixing in the liquid during solidification.

(d) After the metal reaches the eutectic temperature, the metal immediately cools to the heat treatment temperature and solutionizing commences.

(e) During solutionizing, the inter-particle or inter-dendritic eutectic material is assumed to be a homogeneous constituent. The rate of eutectic dissolution can then be directly related to the flux of solute into the primary phase.

Given these assumptions, Fick's second law was then solved for each geometry during both solidification and solutionizing heat treatment. Before describing the details of the numerical analysis to account for diffusion, we will outline the computational sequence for both portions of the analysis.

(a) Solidification

During the solidification portion of the simulation program, the liquid-solid interface is incrementally moved to yield a decreasing volume fraction of liquid. Between each movement increment three steps are implemented. First, solute in the solid is allowed to diffuse for one incremental time interval. Second, the solute within both the solid and liquid phases is integrated to determine the increased composition of the liquid phase. Third, the composition of the interface after the subsequent interface increment is determined using the partition coefficient. To determine the solute concentration at later times, the entire cycle is repeated sequentially.

(b) Solutionizing Heat Treatment

During the solutionizing heat treatment portion of the program, diffusion within the primary solid and interface motion at the eutectic front are taken into consideration. The initial solute and volume fraction of eutectic is determined by the solidification program described above. Two steps are sequentially performed to determine the variation at later times. First, diffusion redistributes solute for one time interval. Second, on the basis of the amount of solute entering the primary solid, the primary solid/eutectic interface is moved in order to conserve solute mass. The two step sequence is repeated, to obtain both solute distribution and volume fraction of eutectic at later times.

(c) Diffusion Model

The diffusion of solute is governed by Fick's laws:

$$\frac{\partial C}{\partial t} = D_s \frac{\partial^2 C}{\partial x^2} \qquad \text{(linear plate-like dendrite)} \qquad \text{(3-a)}$$

$$\frac{\partial C}{\partial t} = D_s\left(\frac{\partial^2 C}{\partial r} + \frac{2}{r} \cdot \frac{\partial C}{\partial r}\right) \text{(spheroidal primary solid particle)} \qquad \text{(3-b)}$$

In these equations, C represents the solute concentration, t is time, and x and r are the spatial coordinates of a linear and spherical coordinate system, respectively. The diffusion coefficient of solute, D, in this formulation is assumed to be independent of solute concentration. The value of D for Al-Cu alloys was deduced

from the data presented in reference (8) and is given by the following equation:

$$D_s = 0.0072 \exp\left[- \frac{24980}{RT} \right] \qquad (4)$$

where R is the Universal Gas constant and T is the temperature in °K.

In addition to the equations listed above, boundary conditions are necessary for the full solution of the diffusion equations:

(a) Linear Plate-like Model

$$\frac{\partial C}{\partial x} = 0 \qquad x = 0,\ t = t \qquad (5\text{-a})$$

$$C = kC_L \qquad \text{at } x = M(t),\ t = t \qquad (5\text{-b})$$

(b) Spherical Particle Model

$$\frac{\partial C}{\partial r} = 0 \qquad r = 0,\ t = t \qquad (6\text{-a})$$

$$C = kC_L \qquad \text{at } r = M(t),\ t = t \qquad (6\text{-b})$$

In addition for the solutionizing portion of the program, a mass balance at the primary solid/eutectic interface yields the last boundary equation:

$$\frac{\partial M}{\partial t} C_L(1-k) = D_s \frac{\partial C}{\partial x, r} \qquad \text{(linear model and spherical model)} \qquad (7)$$

In the above equations, M represents the spatial location of the interface which is a function of time.

In order to solve Fick's second law with the accompanying boundary conditions enumerated above, it is necessary to reformulate the mathematical equations in finite difference form. In addition, it is convenient to employ dimensionless spatial and time variables in the analysis as listed below:

$$t^* = t/t_f \qquad (8\text{-a})$$

$$x^* = x/l_o \; ; \; r^* = r/r_o \qquad (8\text{-b})$$

where r^*, x^* and t^* are dimensionless position and time while t_f, l_o and r_o are the local solidification time and one half of the segregate spacing, respectively. Using these two parameters the finite difference form of the diffusion equation is given below:

$$C_j^{n+1} = C_j^n + \frac{D^*\Delta t^*}{(\Delta x^*)^2} (C_i^n - 2\,C_j^n + C_k^n) \qquad (9\text{-a})$$

for the linear coordinate system, and

$$C_j^{n+1} = C_j^n + \frac{D^*\Delta t^*}{(\Delta r^*)^2} (C_i^n - 2\,C_j^n + C_k^n) + \frac{D^*\Delta t^*}{r^*\Delta r^*} (C_k^n - C_i^n) \qquad (9\text{-b})$$

for the spherical coordinate system.

where $D^* = \dfrac{D_s t_f}{\ell_o^2}$

and Δr^*, Δx^* and Δt^* are the dimensionless spatial and time movements. For the compositions, C, the subscripts indicate the spatial node (location) and the superscript defines the iteration number, (time). These equations were utilized in the computational scheme as described previously.

4. Analytical Solutions

An analytical solution, similar to that reported for a dendritic alloy[7] was derived in order to analyze the solutionization of Rheocast alloys. The general solution outlined by Carslaw and Jaeger[11] was used to arrive at the particular solution of interest to this study. Fick's law, equation (3-b), and the following boundary conditions were used:

$$\frac{\partial c}{\partial r} = 0 \quad \text{at } r=0 \quad t=t \tag{10-a}$$

$$C = C_m \quad \text{at } r=r_o \quad t=t \tag{10-b}$$

$$C = C_m^\circ \quad \text{at } r=0 \quad t=t \tag{10-c}$$

and

$$\frac{C - C_m}{C_m^\circ - C_m} = \cos\left(\frac{\pi}{2}\,\frac{r}{r_o}\right) \quad \text{at } r=r \text{ and } t=o \tag{10-d}$$

using these equations and the formulation of Carslaw and Jaeger[11] the following equation was derived after considerable analysis:

$$\frac{g + a}{g_o + a} = 1 - \frac{3^2}{(2\pi^2 - 16)} \sum_{n=1}^{\infty} \frac{1}{(4n^2-1)^2} \left\{1 - \exp\left[-(n\pi)^2 \left(\frac{D_s t}{r_o^2}\right)\right]\right\} \tag{11}$$

where each of the parameters has been previously defined.

5. Results and Discussion

Metallographic examination of the solutionized samples showed a continual change of microstructure with increasing heat treatment time. Figure 13 shows the sequence of microstructures after 0, 1/2, and 10 hours of solution treatment for conventional cast 2024 aluminum base alloy. The non-

treated specimen, Figure 13 (a), has a dendritic structure with a secondary dendrite arm spacing of approximately 45μm. Each dendrite arm is surrounded by a continuous film of second phase and numerous second phase pockets can be observed throughout the structure. After half an hour of heat treatment, Figure 13(b), the dendrite structure is still apparent; however considerable coarsening of the structure has occured due to the dissolution of some interdendritic second phase. Figure 13 (c) shows the microstructure after 10 hours of solutionizing treatment revealing the continued dissolution and the presence of precipitate particles throughout the periphery of the dendrites. The precipitates which form upon cooling from the heat treatment temperature show the extent of solute diffusion into the dendrite bulk. However, as shown in Figure 13 (c), ten hours is insufficient for complete dissolution of the interdendritic second phase.

The microstructures of Rheocast 2024 aluminum base alloy shown in Figure 14 reveal similar characteristics following heat treatment. The three microstructures following 0, 1/2, and 10 hours of heat treatment have decreasing amounts of interparticle second phase. Also for the sample solutionized for 10 hours, a dense precipitate distribution is evident around the periphery of the primary solid particles. For the longest solution time, Figure 14(c), the film of second phase between particles present in the non-heat treated sample, Figure 14(a), has dissolved leaving isolated pockets of second phase at the interstices between particles. In contrast with the dendritic structure, the scale of the Rheocast structure is coarser with

a measured average particle diameter of approximately 114μm despite the fact that the ingots for both processing conditions experienced nearly equivalent cooling rates upon solidification. In fact, comparison of the primary dendrite spacing of the conventional cast aluminum alloy and the primary solid particle size provided much closer agreement as previously noted in Figures 3 and 5.

Figure 15 shows the experimental measured variation in the volume fraction of interdendritic phase as a function of time for the Rheocast and the conventional cast 2024 aluminum base alloy. Although the curves for each processing mode exhibits similar characteristics, the initial volume fraction for the Rheocast alloy is only 0.062 whereas the initial volume fraction for the dendritic material is 0.075. After 50 hours, however, both materials retain approximately 0.014 volume fraction of inter-dendritic or inter-particle phases. Since little change is detected between the amount of interdendritic and inter-particle phases after heat treatment for 10 to 50 hours, one can conclude that 0.014 is the equilibrium fraction at the heat treatment temperature of 515°C.

The change in the amount of non-equilibrium phase with time was modelled using the analytical techniques previously described. Figure 16 shows the results of the diffusion simulation for the solidification and solutionization of dendritic 2024 aluminum alloy. The analytical curve which is also plotted was obtained from equation (11). The general shape of both the simulation and the analytical curves is similar; however, the analytical curve predicts that at any dimensionless time more dissolution

will occur than is predicted by the numerical technique. Of the two curves, the numerical simulation technique agrees most closely with the experimental points, particularly at short times (less than one hour). However, after one hour ($t^* \cong .5$) both predictive models yield a volume fraction of second phase which is considerably lower than the experimental values. A similar plot is shown in Figure 17 which describes the solution kinetics of Rheocast 2024 aluminum alloy. The dimensionless time axis for this plot is shifted one decade with respect to the axis of Figure 16. Again the numerical simulation technique provides best agreement with the measured data and each model yields a curve which falls beneath the data at real times in excess of one hour ($t^* \cong 10^{-1}$). One important implication of these findings is that for a given value of dimensionless time the spherical Rheocast structure solutionizes faster than the plate-like dendritic structure.

During solidification of 2024 aluminum base alloy $CuAl_2$, $CuMgAl_2$, (CuFe Mn) Al_6 and (Fe Mn)$_3$ Si_2 Al_{15} second phases solidify in the interdendritic regions (12). The composition of the second phases before and after solution heat treatment was qualitatively established by Secondary Electron Imaging, elemental x-ray maps and comparison of our findings with data reported above. Figure 18 and 19 show the SEI's and the associated x-ray elemental maps of copper, iron and magnesium of the as cast alloy. The second phase particle in Figure 18(a) is probably $CuMgAl_2$, whereas the horseshoe shaped particle in Figure 19(a) is $CuAl_2$. Some of the lighter colored phases in Figure 19(a) show concentration of both copper and iron and are probably the (CuFeMn)Al_6 phase noted above.

During short solutionizing heat treatment time magnesium diffuses rapidly from the second phase, leaving behind nearly pure $CuAl_2$ particles and iron-rich second phases. Furthermore, some eutectic $CuAl_2$ lamellae appear to agglomerate. Figure 20(a) shows the second phase particles in the Rheocasting ingot after a solution heat treatment of 1/2 hr. A larger magnification of the agglomerated $CuAl_2$ second phase particle, $\alpha + CuAl_2$ eutectic structure and an iron-rich phase, perhaps $(FeMn)_3Si_2Al_5$, is also shown in Figure 20 with the corresponding elemental x-ray maps. It is apparent that the large agglomerate and the lamellae eutectic are copper-rich, while the gray second phase particle has a relatively high iron concentration.

With longer solutionization times most of the $CuAl_2$ second phase particles disappear while the iron-rich phases do not. Figure 21 shows the continued presence of some $CuAl_2$ and iron copper-rich second phase, perhaps $(CuFeMn)Al_6$, after a solution heat treatment of 10 hrs.

One important finding of the experimental measurements and the computer simulation, is that the response of a metal to solutionizing treatment is strongly influenced by the geometry of the primary solid phase. Unfortunately, this is not clearly evident in Figure 15 because although the geometrical features of each microstructure is different, the particle size of the Rheocast material is more than twice as large as the secondary dendrite arm spacing of the conventional cast metal.

When plotted on dimensionless coordinates, the higher dissolution rate of the second phases in the spherical morphology is clearly evident - compare the curves of Figures 16 and 17. This

increase in dissolution rate is due to the spherical geometry which provides a larger surface area of the second phase/primary solid interface per unit volume than that for any other simple geometrical shape. This finding would probably be extended to equiaxed structures where the final solidification morphology resembles the Rheocast structures. However, it is also clear from the diagrams presented that in order to exploit this advantage of spherical growth forms it is essential to maintain a particle size or grain size which is smaller than the primary dendrite arm spacing of a conventionally cast metal. Otherwise, the increased diffusion distance of the Rheocast will offset the geometrical advantages.

Of the two simulation methods employed, analytical and numerical, the analytical technique provided a faster rate of solutionization for both growth morphologies investigated. This difference, however, is not large and is clearly understandable considering the assumptions employed in the derivation of equations (1) and (11). For both the flat plate and spherical models an initial sinusoidal distribution of solute was assumed prior to diffusion. In contrast, the numerical solution determined the non-equilibrium solute distribution by incorporating diffusion in the solid into the solidification model.

V. ECONOMIC ASPECTS OF MACHINE CASTING

The general aim of this portion of the investigation was to calculate the economic aspects of the new high temperature alloy machine casting process. A cost analysis model was developed earlier (1) to project and compare cost per piece with established methods of manufacture. This costing technique has been revised to include realistic estimates of capital equipment cost for the Rheocasting and the Thixocasting portions of the machine casting operation. Furthermore, recent results on die cost and die life obtained in the M.I.T. program on machine casting (13) are included in the analysis presented herein. A conventionally investment cast part, the hammer on the M-16 rifle, is used as an example for machine casting cost analysis.

A. Cost Breakdown

Cost associated with the manufacture of parts by the new machine casting process is subdivided into two sequence of operations:

(a) Melting and Rheocasting - billets of appropriate diameter which fit in the shot sleeve of a cold chamber die casting machine are Rheocast.

(b) Thixocasting - the Rheocast billets are rheated via induction, softness tested and machine cast in the die casting machine.

The sequence of manufacturing operations is broken down into direct material and direct labor costs. Some of the usual manufacturing overhead costs (e.g. utilities, employee benefits, service and maintenance, etc.) are considered as part of direct materials and labor costs. The other manufacturing overhead costs (e.g. administration, marketing, research, sales, profits, etc.) are unique to the manufac-

turer, hence are not included in this cost analysis. The capital equipment cost for Rheocasting and Thixocasting are calculated and amortized over the estimated life cycle of the components. An important input in the cost analysis is the cost and life of the machine components, especially die life. Information generated in a pilot plant machine casting operation for Thixocasting of a similar part at M.I.T. (13) was included in this cost analysis. Finally, it should be noted that finishing and inspection costs are not included in the estimates of cost per piece.

In the model, the amortized cost of equipment for the Rheocasting and the Thixocasting operations are calculated separately. The amortized equipment cost for Rheocasting is used in estimating the cost of Rheocast metal (in this case, 8620 low alloy steel) ingots delivered to the Thixocasting plant. Direct materials, machine component and labor costs incurred in the Thixocasting operations are then estimated from work sheets which permit calculation of:

1. Estimated Rheocast Metal Cost - which uses the Rheocasting cost and the basic alloy cost,
2. Estimated Metal Cost per Piece - which takes the number of pieces per die and metal used in the biscuit, gates, runners and overflows into consideration, and
3. Thixocasting (Reheating and Die Casting) Cost per Piece - which includes labor, material and machine components costs, including die cost and die life.

B. Amortized Capital Equipment and Rheocasting Cost of Low Alloy Steel

Capital equipment cost for continuous Rheocasting was developed from earlier estimates made in this program (1) and from information received from the M.I.T. investigators (13). Estimated cost of Rheo-

casting steel ingots was then calculated using direct material and labor charges and the amortized capital equipment cost.

ESTIMATED CAPITAL EQUIPMENT COST FOR CONTINUOUS RHEOCASTING*

Description	Purchase Price and Installation	Write-Off Period (years)	Annual Depreciation ($/year)
Two continuous Rheocasting apparatuses	40,000.00	10	4000.00
Two 500 lb. melt stations	10,000.00	10	1000.00
Two 100KW induction power supplies	100,000.00	15	∿6667.00
Four 20KW induction power supplies	60,000.00	15	4000.00
Mold system to collect Rheocast Ingots	20,000.00	10	2000.00
Instrumentation	10,000.00	10	1000.00
TOTAL	$240,000.00		$18,667.00

* The costs are estimated for two continuous Rheocasting units, one of which would be in continuous production during the time period used for estimation of Rheocasting cost/lb.

ESTIMATED COST OF RHEOCASTING STEEL INGOT/lb.

	$/lb.
Melting Cost (1)	0.10
Materials and Preparation (2)	0.022
Labor with Overhead and Fringe Benefits (2)	0.075
Gas Shield, Mold Materials, etc. (2)	0.01
Capital Equipment Cost (2)	0.006
TOTAL	0.213

(1) Melting cost is for a 500 lb. holding furnace and includes furnace linings, melt losses and utilities.

(2) These estimates are from Reference (13) and are based on three shift continuous operation of one of the two continuous Rheocasters seven days a week and fifty weeks a year. Rheocast ingot metal yield at 80% efficiency is ∿ 3,360,000 lbs/year. Note that capital equipment cost of the two Rheocasters and associated equipment, shown in the previous page, is included in the above.

The amortized equipment cost for the Thixocasting operation is given below:

ESTIMATED CAPITAL EQUIPMENT COST FOR THIXOCASTING

Description	Purchase Price and Installation	Write-Off Period (years)	Annual Depreciation ($/year)
One 50 KW induction power supply for slug reheating	$26,000.00	15	1,733.00
One 400 ton die casting machine	80,000.00	12	6,667.00
Two Mold Bases (die holders)	18,000.00	15	1,200.00
Slug Reheat Station	10,000.00	10	1,000.00
Automatic System for Mold Wipe and Lubricant	10,000.00	10	1,000.00
TOTAL	$144,000.00		$11,600.00

C. Machine Casting Cost of the M-16 Hammer

The work sheets are used below to estimate the cost for manufacture of the hammer in the M-16 rifle.

WORK SHEET #1 - ESTIMATED METAL COST PER PIECE

Alloy Cost $/lb. + (Melting and Rheocasting Cost) $/lb. =

$$\frac{0.17}{\text{Rheocast Metal Cost \$/lb.}} + \frac{0.213}{0.383} =$$

Alloy cost is for 8620 low alloy steel.

WORK SHEET #2 - ESTIMATED METAL COST PER PIECE

A. Net Metal Cost per Shot

Pieces/Die x lbs/Piece + lbs/G,R,B,&O* =

16 x 0.07 + 1.49 =

lbs/shot x Rheocast Metal Cost/lb = Gross Cost - lbs x (G,R,B, &O) x Scrap Price

2.61 x 0.383 = 1.00 - 1.49 x 0.9 x 0.17

= Net Cost

+ ~ $0.77/lb.

B. Net Metal Cost Per Piece

Net Cost ÷ Pieces/Die = Net Cost/Piece

0.77 ÷ 16 = ~$0.048

* G,R,B,&O designate gates, runners, biscuit and overflows.

WORK SHEET #3 - THIXOCASTING (REHEATING AND DIE CASTING) COST PER PIECE

Labor (O.H. fringe + utilities) ÷ (Shots/hr x Pieces/die)

$15/hr ÷ (90 x 16)

+ Die Cost/Piece + Shot Sleeve Cost/Piece + Plunger Tip, Runner pads and Center block/piece

+ 0.145 + 0.0025 + 0.014

+ Reheat Crucible Lubricant Cost/Shot ÷ Pieces/die = Cost/Piece

+ 0.16 ÷ 16 = ∿ 0.182/piece

(1) Shots/hr includes die set-up time, 75% efficiency in a three shift operation.

(2) Die cost and die life estimates were obtained from Reference (13). These include the following:

(a) Die material cost (Cu-1%Cr-1%Zr alloy) at $4.00/lb. Total die material cost for the sixteen cavity die, 140 lbs, is $560.00

(b) Initial tooling cost for the sixteen cavity die is estimated at $22,000.00

(c) Die life before EDM retooling ∿ 5000 shots

(d) Nine Subsequent EDM retooling with a life of ∿ 5000 shots each at a cost of $10,400.00 per retooling

$$\text{Die Cost/piece} = \frac{\text{total die cost}}{\text{pieces/die x total die life}} = \frac{\$116,160.00}{16 \times 50,000}$$

(3) $$\text{Shot Sleeve Cost/piece} = \frac{\text{cost of shot sleeve}}{\text{pieces/die x shot sleeve life}} = \frac{\$400.00}{16 \times 10,000}$$

$$= 0.0025$$

(4) Plunger Tip, Runner Pads and Center Block/piece =

$$\frac{\text{cost}}{\text{pieces/die x life}} = \frac{\$1,100.00}{16 \times 5000} = 0.014$$

ESTIMATED MACHINE CASTING COST OF M-16 HAMMER per PIECE

1.	Estimated metal (8620 low alloy steel) cost per piece from Work Sheet #2. This estimate includes Rheocasting cost from Work Sheet #1.	$0.048/piece
2.	Estimated Thixocasting cost from Work Sheet #3. This includes $0.145/piece of die cost	$0.182/piece
3.	Capital Equipment Cost for Thixocasting per piece. Amortized capital equipment cost is ∿$11,600.00/year. Assuming a 90 shots/hr rate (75% efficiency) at 20 hrs per day, five days a week and fifty weeks per year, a total number of 450,000 shots are calculated per year. Each shot produces 16 castings.	$0.0016/piece
	TOTAL Cost	∿$0.23/piece

Note that die cost ($0.145/piece) is a substantial percentage (63%) of the total cost per piece. Finally, it should be noted that the projected cost above does not include cutting, grinding, finishing and inspection operations. Estimated yield would depend on the severity of inspection criteria. The latter should be relatively high for an automated machine casting operation.

The investment cast hammer for the M-16 rifle was procured for approximately $1.00/piece in the early 70's by the Department of Defense. It would be difficult to directly compare the cost of machine casting with investment casting due to several unknown factors including; finishing cost, inspection and certification cost, yield after each inspection step and manufacturer's overhead and profits. However, it does appear that even with inflation costs of the past few years, the projected machine casting cost per piece is reatively low.

VI. CONCLUSIONS

1. Various model, low and high temperature continuous slurry producers and a transparent model die casting machine were designed, built and operated.

2. The structures of continuously Rheocast slurries of a non-metal NH_4Cl-H_2O, and a variety of metallic alloys including Sn-15% Pb, 2024 aluminum base alloy, 905 copper base alloy, 304 stainless steel, 440C stainless steel and X-40 cobalt base alloy were studied.

3. The important relationships between process variables and the structure of the continuously produced slurries were established. In general, average cooling rate has the most pronounced effect on the slurry structure. Increasing the average cooling rate makes the primary solid particles more uniform and smaller in size. Furthermore, primary dendrite arm spacings in conventional castings and primary particle size in the slurries are of the same order of magnitude if average cooling rates during solidification are identical.

4. The effect of cast (Rheocast) structures on microsegregation, solution heat treatment response, and mechanical properties of the alloys were studied. It was found that:

(a) Water quenched slurries consistently showed relatively flat elemental composition profiles of alloying elements in the primary solid particles with abrupt changes at their boundaries.

(b) During solution heat treatment significant solute redistribution, dissolution and reprecipitation of second phases occurs. In general, solution heat treatment results in improvement in properties similar to conventionally cast structures.

(c) A computer solution heat treatment model was developed and verified by experiments. The important finding from this work was

that Rheocast structures solutionize much faster than conventional dendritic structures. The increase in dissolution rate of second phases is due to the spherical geometry of the primary particles in Rheocast ingots.

(d) In general, solution heat treatment improves the properties of Rheocast ingots, e.g. room temperature compressive yield strength of 440C stainless steel increased from 150,000 psi to 240,000 psi after a 5 hour solution heat treatment at ∿1300°C. In the absence of porosity Rheocast ingots of X-40 colbalt base alloy exhibited tensile and stress rupture properties equivalent to the conventionally cast material.

5. Experiments on the transparent model die casting system showed that the mode of die filling can be related to dimensionless numbers. Reduced porosity, turbulence, and vorticity were observed when the die cavity filled with a solid front. It is anticipated that as the volume of fraction of solid in a Rheocast slurry increases solid front fill (reduced porosity in the casting) can be achieved at relatively high ingate velocities.

6. A cost analysis model for Rheocasting and Thixocasting was developed. The model permits cost breakdown for manufacture of parts by the new machine casting process. An example is given for machine casting cost of a conventionally investment cast part.

VII. REFERENCES

1. R. Mehrabian , D. G. Backman, Y. V. Murty, R. J. Lauf, S. D. E. Ramati and S. Hong, "Machine Casting of Ferrous Alloys," Semi-annual Technical Report, ARPA Contract No. DAAG46-76-C-0023, 1 October to 31 March 1976, prepared for Army Materials and Mechanics Research Center, Watertown, Mass.

2. R. Mehrabian, D. G. Backman, Y. V. Murty, G. J. Abbaschian, S. D. E. Ramati, S. Hong and R. J. Lauf, "Machine Casting of Ferrous Alloys," Semi-annual Technical Report, ARPA Contract No. DAAG46-76-C-0023, 1 April 1976 to September 30 1976, prepared for Army Materials and Mechanics Research Center, Watertown, Mass.

3. R. Mehrabian, S. D. E. Ramati, G. J. Abbaschian, D. G. Backman and Y. V. Murty, "Machine Casting of Ferrous Alloys," semi-annual Technical Report, ARPA Contract No. DAAG46-76-C-0023, 1 October 1976 to 31 March 1977, prepared for Army Materials and Mechanics Research Center, Watertown, Mass.

4. P. A. Joly and R. Mehrabian, J. of Materials Science, Vol. 11, 1976, p. 1393.

5. L. F. Schulmeister, J. D. Hostetler and C. C. Law, "Machine Casting of High Temperature Alloys For Turbine Engine Components," Final Report, ARPA Contract No. DAAG 46-76-C-0029, 1 March 1976 to 30 May 1977, prepared for Army Materials and Mechanics Research Center, Watertown, Mass.

6. J. M. Oblak and W. H. Rand, Metallurgical Trans., Series B, Vol. 7B, 1976, p. 705.

7. S. N. Singh and M. C. Flemings, Trans TMS-AIME, 1969, Vol. 245, pp. 1803-1809.

8. S. N. Singh, B. P. Bardes and M. C. Flemings, Metallurgical Transactions, 1970, Vol. 1, pp. 1383-1388.

9. R. A. Tanzilli and R. W. Heckel, Trans TMS-AIME, 1969, Vol. 245, pp. 1363-1366.

10. V. V. Teleshov and V. S. Zolotorevsky, Tsvetnaya Met., 1967, Vol. 5, pp. 136-141.

11. H. S. Carslaw and J. C. Jaeger, Conduction of Heat in Solids, Clarendon Press, Oxford, 1959.

12. L. F. Mondolfo, Aluminum Alloys: Structure and Properties, Butterworth & Co., Ltd, London, 1976.

13. J. F. Boylan, R. L. Bye and M. C. Flemings, M.I.T.,

    private communications.

TABLE I

EFFECT OF PROCESS VARIABLES

ON STRUCTURE AND VISCOSITY

AVG. SHEAR RATE	AVG. COOLING RATE	PARTICLE SIZE	ENTRAPPED LIQUID	VISCOSITY
↔	↑	↓	↑	↑
↑ (1)	↔	↓	↓	↓
↑ (2)	↔	↔	↓	↓

(1) Low Cooling Rates up to $\sim 0.5°C.sec^{-1}$

(2) At Cooling Rates $> 0.5°C.sec^{-1}$

} These cooling rates are for the Sn-15%Pb alloy.

↑ denotes an increase

↓ denotes a decrease

↔ denotes no change

TABLE II

Mechanical Properties of X-40 Cobalt Base Alloy

Property	As-Rheocast	Investment Cast	Design Minimum
0.2% Tensile Yield Strength (KSI)	77	76	50
Ultimate Tensile Strength (KSI)	96	108	83
% Elongation	3.0	7	4.0
Stress-Rupture at 790°C and 30 KSI following isostatic pressuring at 1200°C and 15,000 psi	58.6	60	--

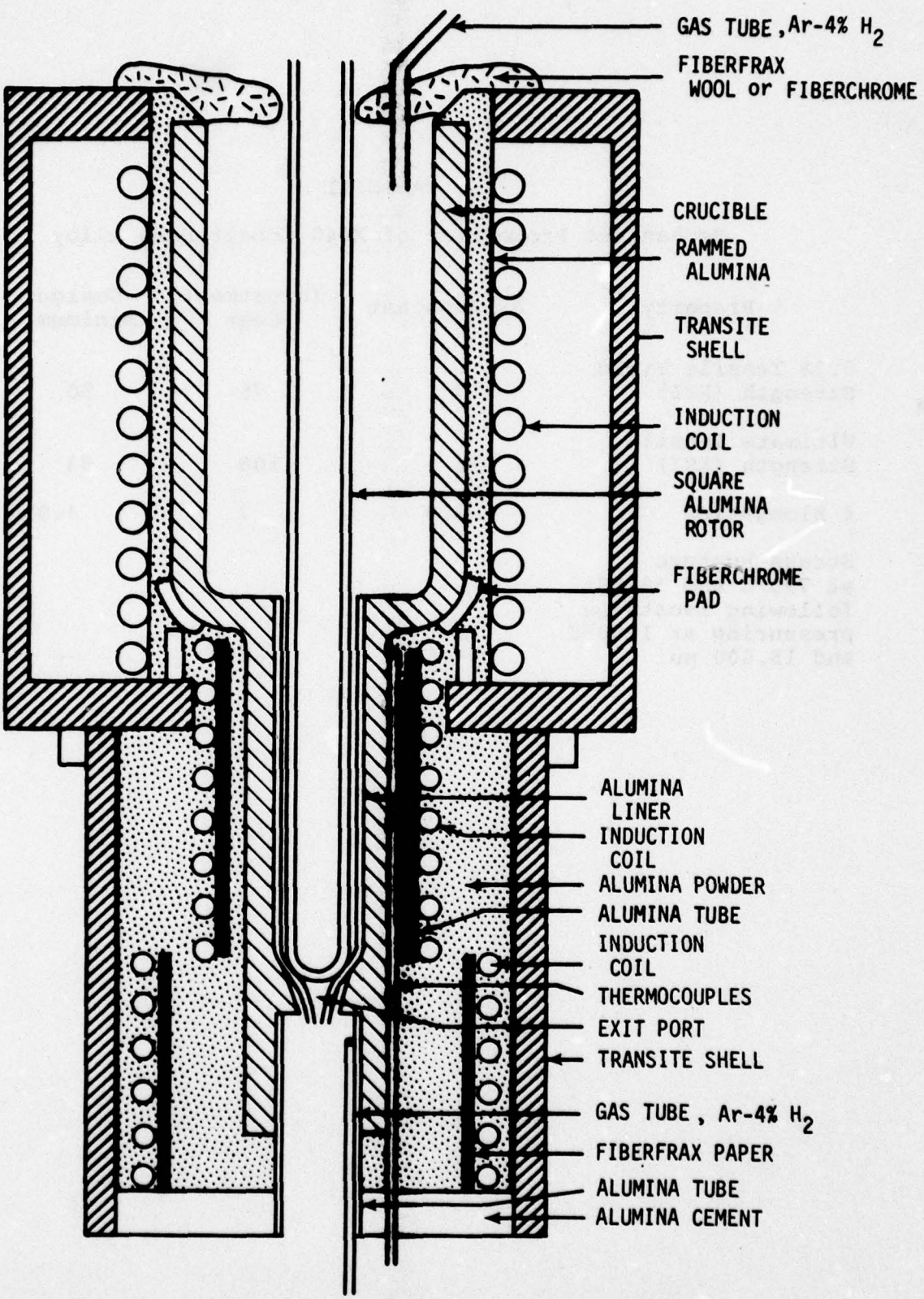

Figure 1. Schematic illustration of the high temperature continuous slurry producer.

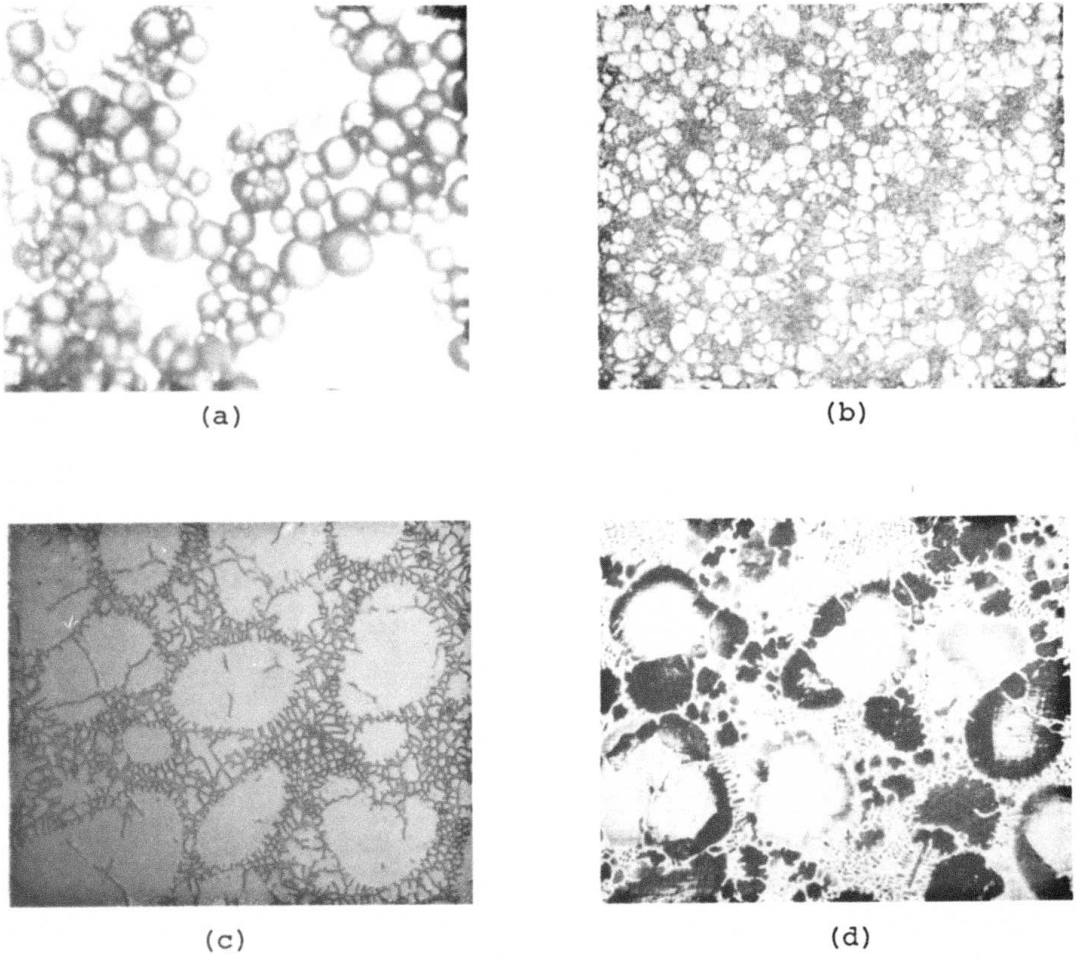

Figure 2. Microstructures of continously produced slurries (a) NH_4Cl-H_20, (b) Sn-15% Pb, cooling rate ≃ 5.52°C.sec^{-1}, shear rate ≃ 650 sec^{-1}, (c) and (d) are X-40 cobalt base superalloy and 440C stainless steel, respectively, cooling rate ∿ 0.6°C sec^{-1}, shear rate ∿ 600 sec^{-1}.

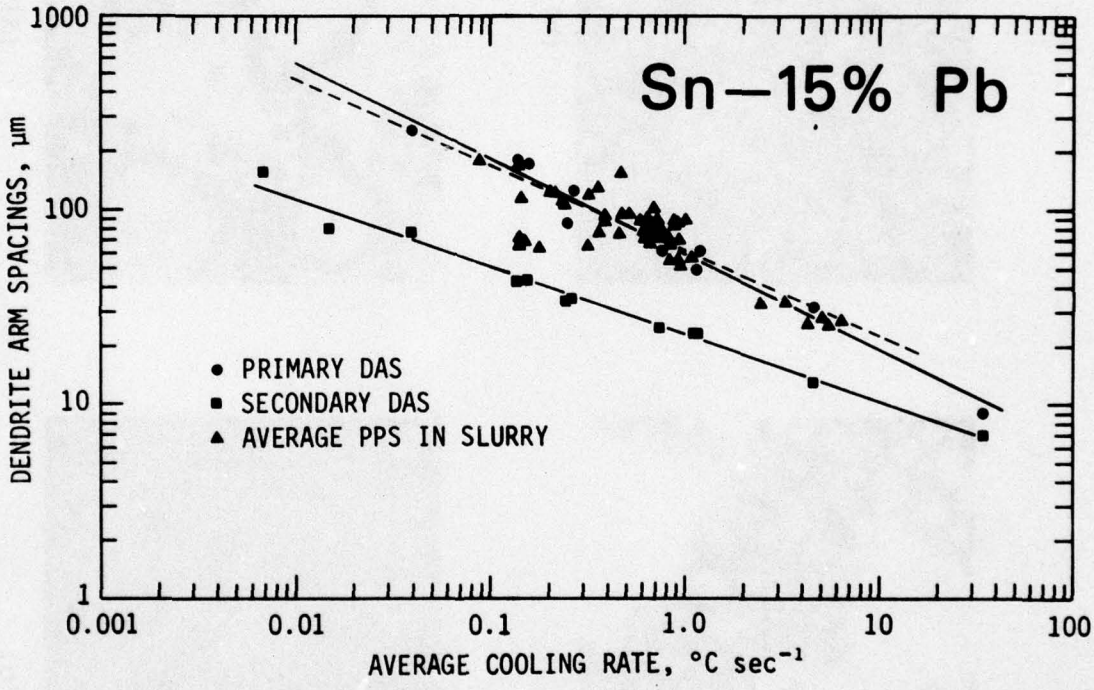

Figure 3. Variation of dendrite arm spacings, DAS, in conventionally cast, and variation of primary solid particle size, average PPS, in continuously produced slurry of Sn-15% Pb alloy with cooling rate during solidification.

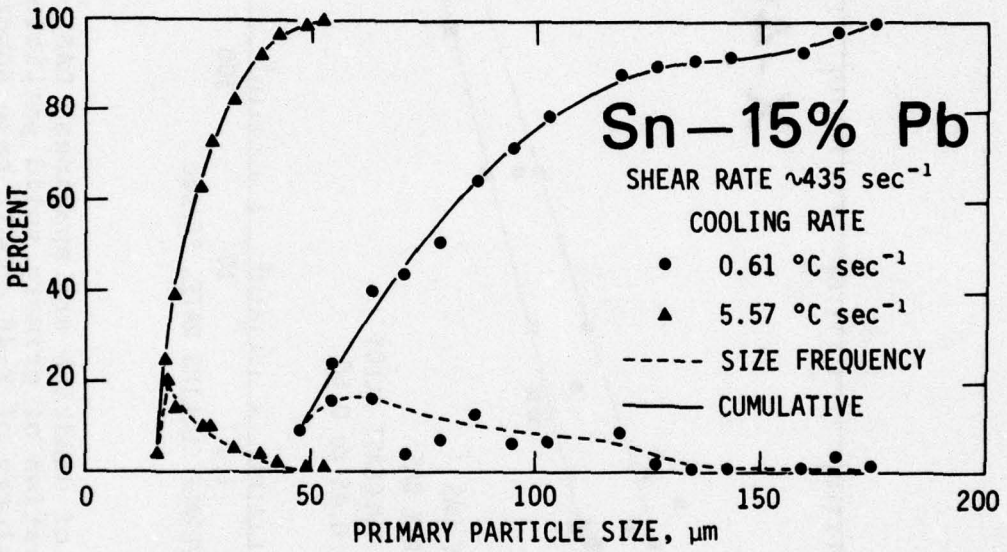

Figure 4. Effect of cooling rate, at a given shear rate of ∿ 435 sec^{-1}, on percent size frequency and cumulative percent of primary solid particles in continuously produced slurries of Sn-15%Pb alloy.

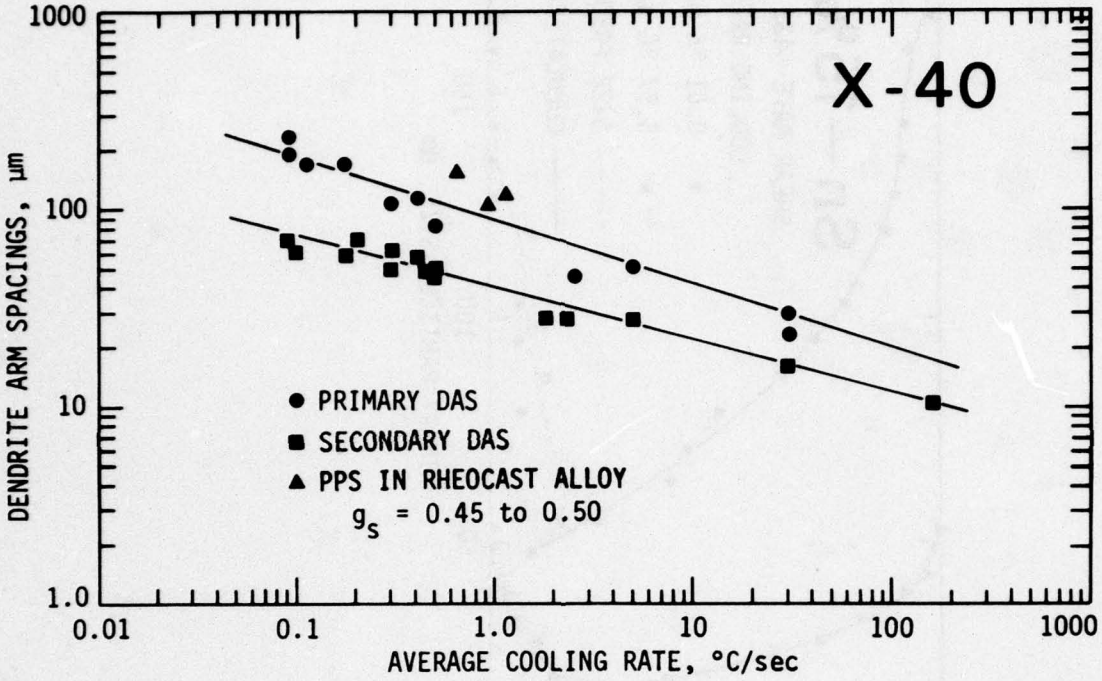

Figure 5. Variation of dendrite arm spacings, DAS, in conventionally cast, and variation of primary solid particle size, p.p.s., in continuously produced slurry of X-40 cobalt base superalloy with average cooling rate during solidification.

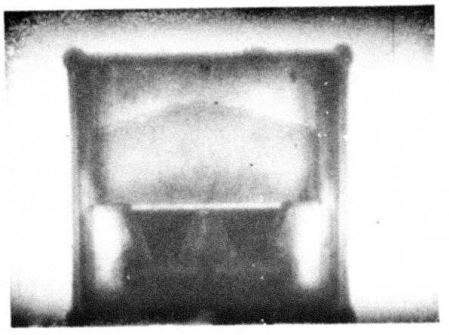

(a)

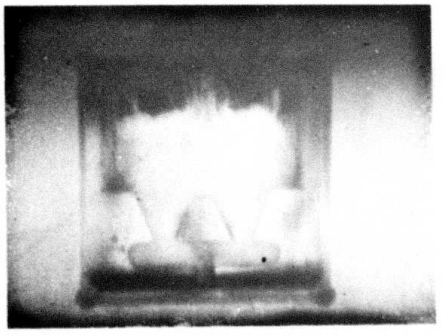

(b)

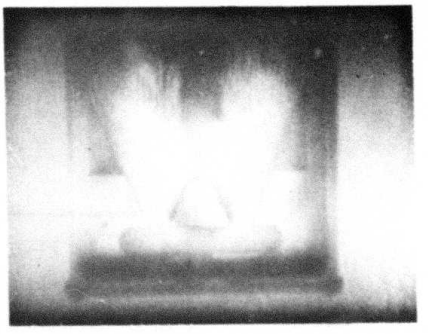

(c)

Figure 6. Photographs showing the three modes of filling for the flat plate die cavity. (a) Solid front fill of S-600 standard viscosity fluid at an ingate velocity of 12 feet per second, (b) transitional fill of standard HV oil at an ingate velocity of 100 feet per second, and (c) atomized fill of standard HV oil at an ingate velocity of 150 feet per second.

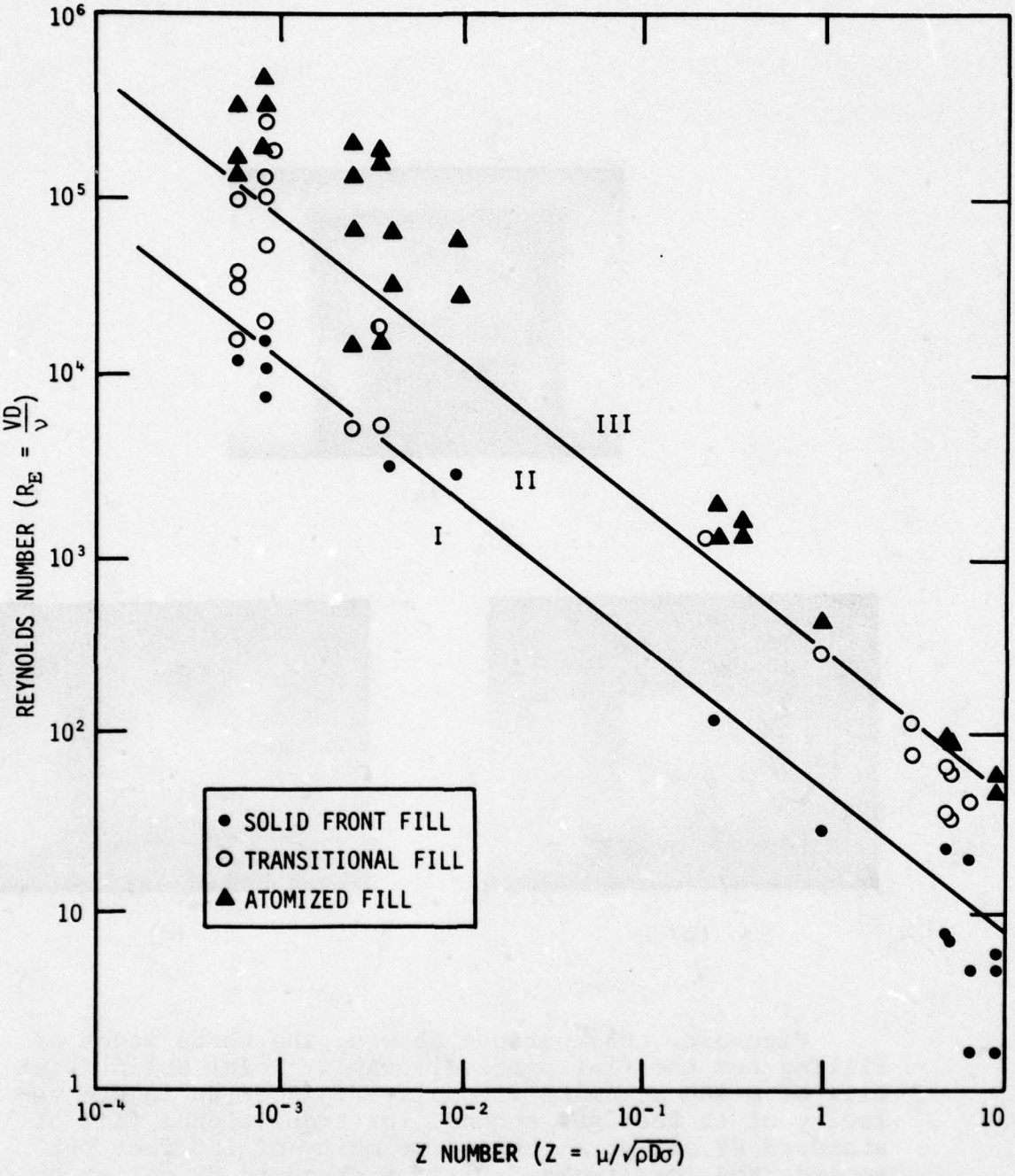

Figure 7. Experimental data obtained, in both of the casting cavity designs, presented in terms of the Reynolds number versus the Z number. μ, ν, σ and ρ are viscosity, kinematic viscosity, surface tension and density of the charge material, respectively. V is ingate velocity and D represents the hydraulic diameter of the gate. This plot permits prediction of the mode of die filling.

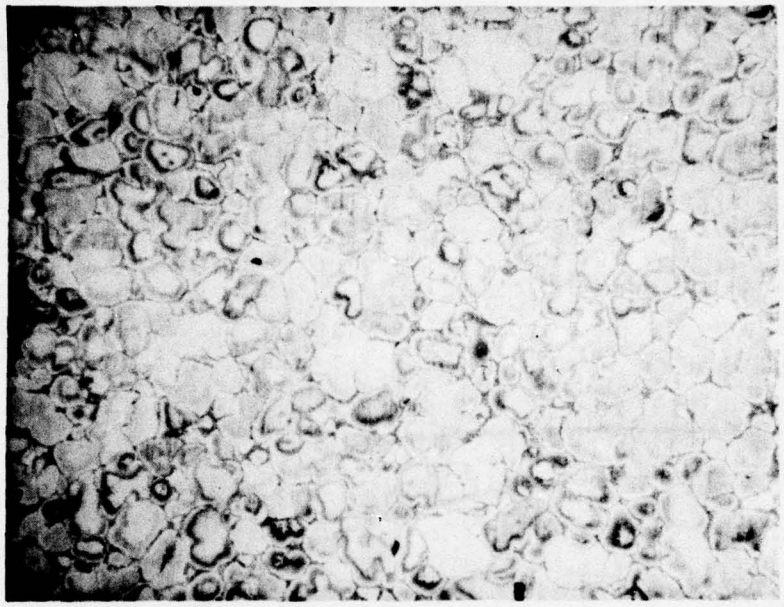

(a)

(b)

Figure 8. Ingot microstructures of continously produced semi-solid alloy; (a) 440C stainless steel and (b) X-40 cobalt base superalloy. Samples were slowly cooled in ingot molds. Magnification 65X.

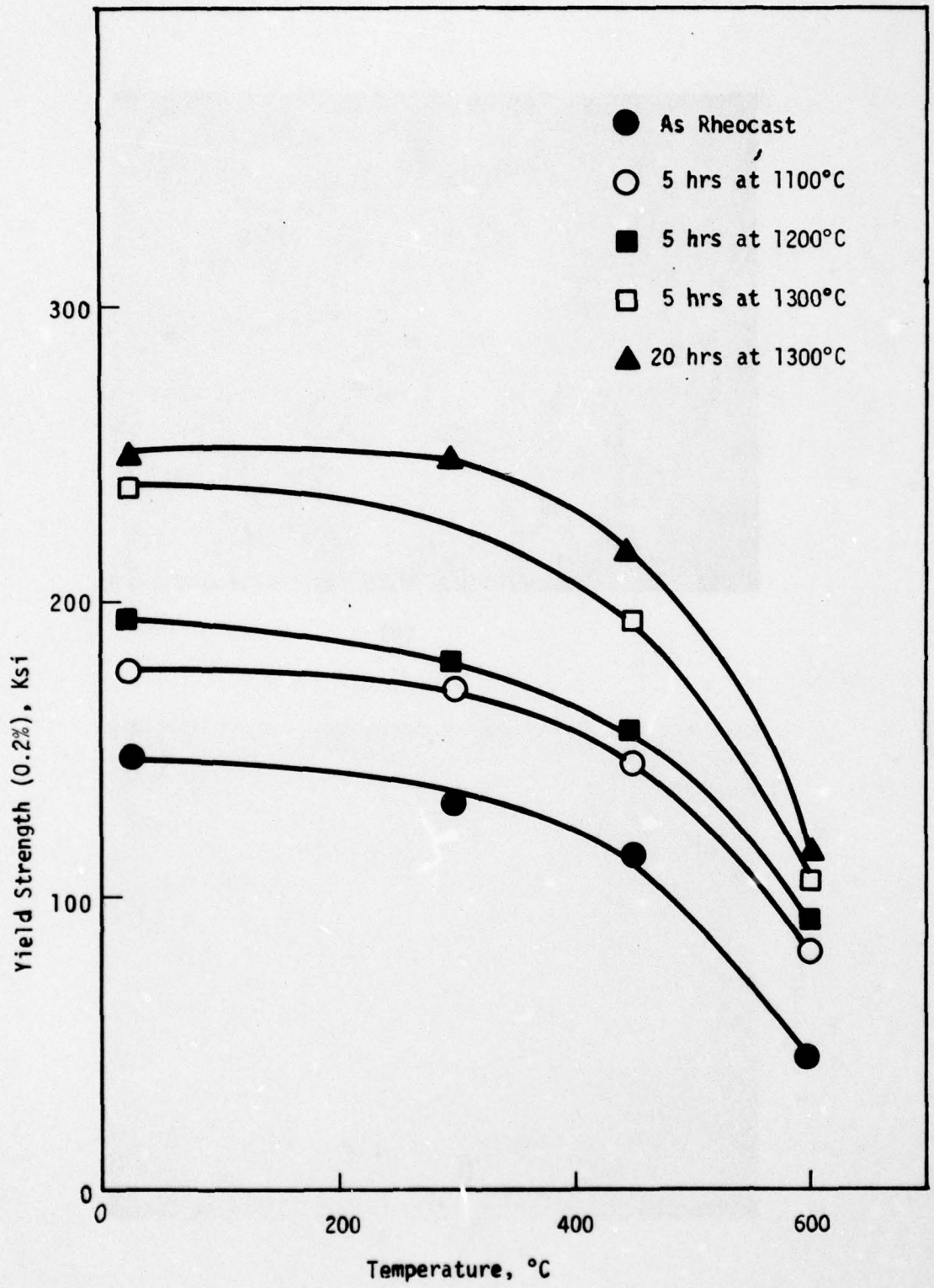

Figure 9. Measured compressive yield strength of as-Rheocast and homogenization heat treated 440C stainless steel as a function of temperature.

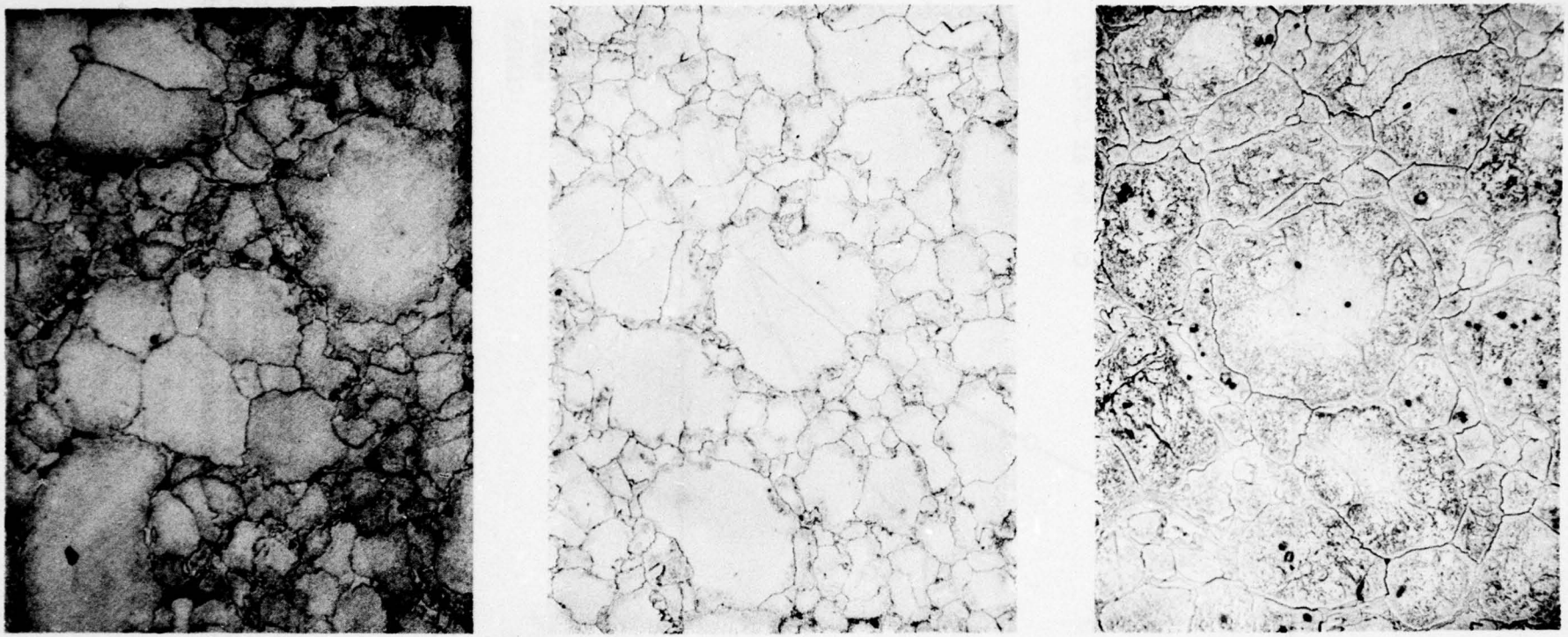

(a) (b) (c)

Figure 10. Microstructures of solution heat treated X-40 cobalt base alloy Rheocast ingots, magnification 200X. (a), (b), and (c) are from specimens solutionized for 5 hours at 1100°C, 1200°C, and 1300°C, respectively.

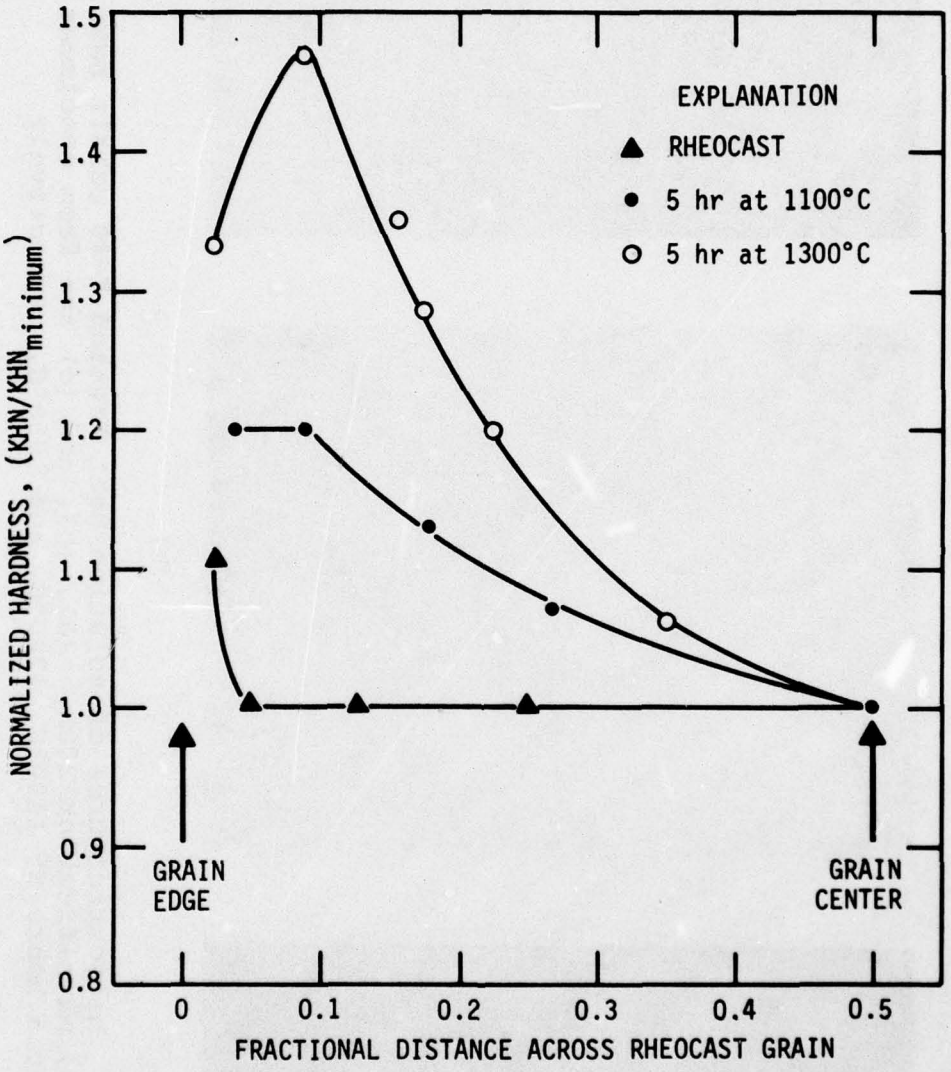

Figure 11. Measured variation of microhardness, normalized as the ratio of Knoop hardness number at a given location against the minimum value, across the Rheocast grain of X-40 cobalt base alloy in as-Rheocast and homogenized heat treated conditions.

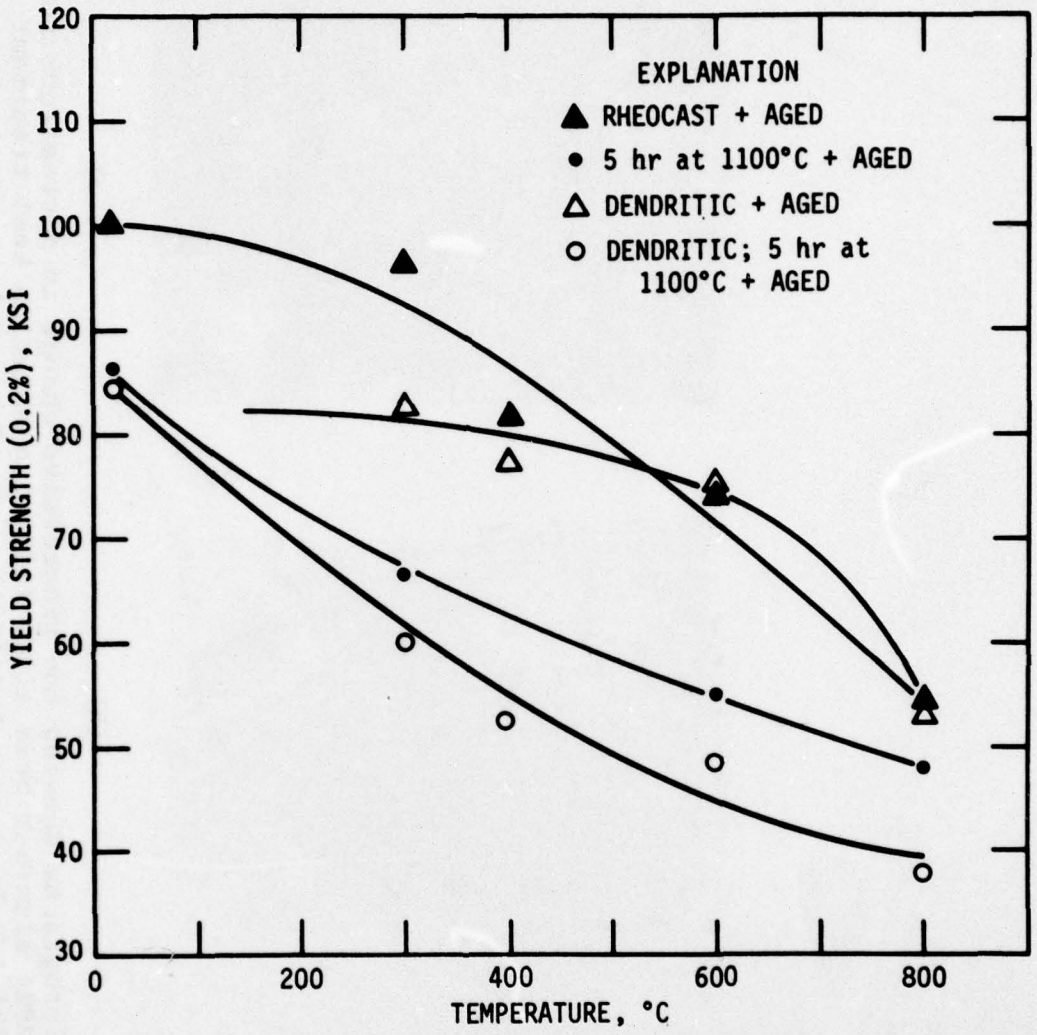

Figure 12. Measured compressive yield strength for dendritic and Rheocast X-40 cobalt base superalloy after two different heat treatments. (1) Aged at 700°C for 50 hours; (2) homogenized (5 hours at 1100°C) plus aging at 700°C for 50 hours.

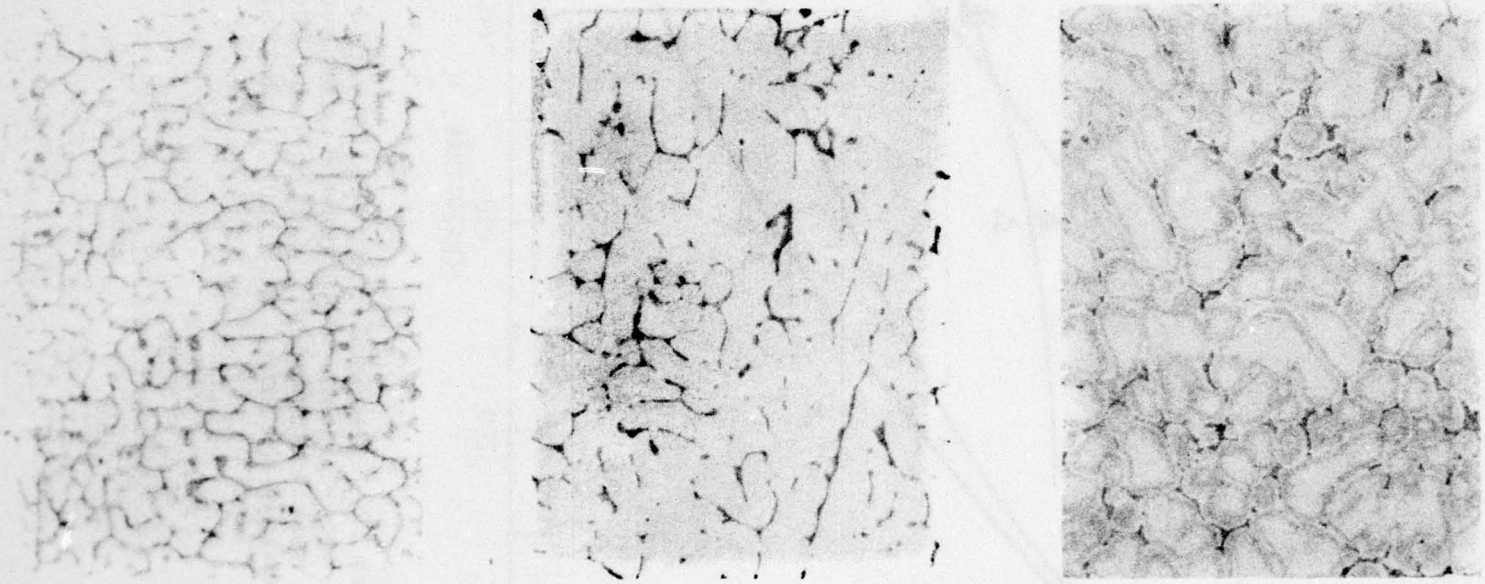

(a) (b) (c)

Figure 13. Photomicrographs showing the progressive change in microstructure of conventionally cast 2024 aluminum base alloy following solution heat treatment at 515°C; (a) as cast, (b) 1/2 hour heat treatment, (c) 10 hours heat treatment; magnification: 100X.

(a)

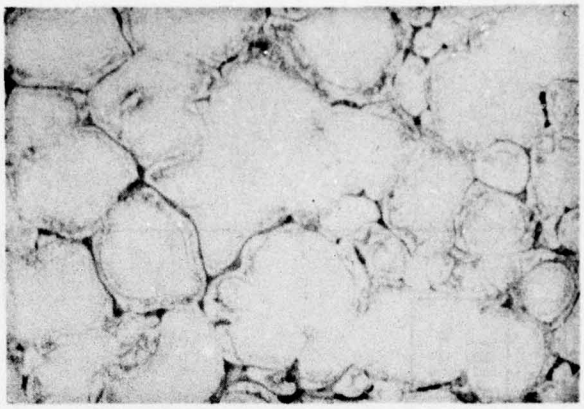

(b)

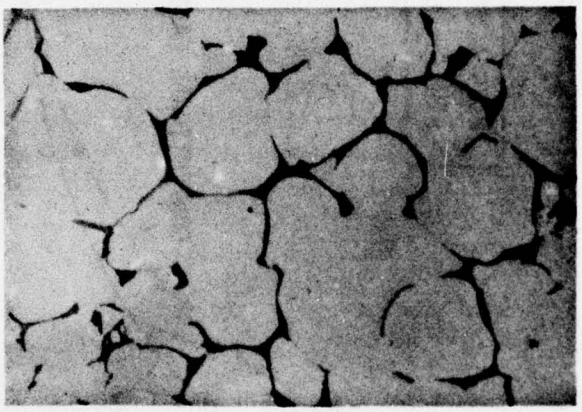

(c)

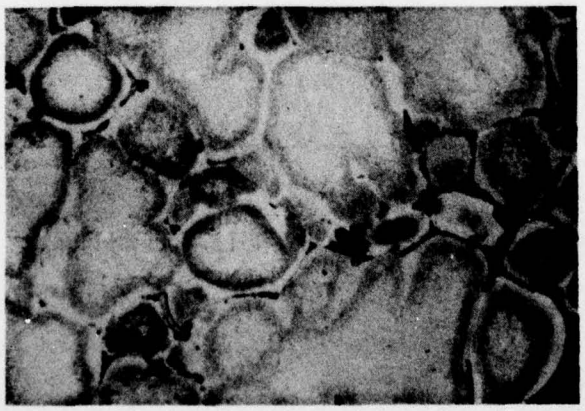

Figure 14. Photomicrographs showing the progressive change in microstructure of Rheocast 2024 aluminum base alloy following solution heat treatment at 515°C; (a) as Rheocast, (b) 1/2 hour heat treatment, (c) 10 hours heat treatment; magnification: 100X.

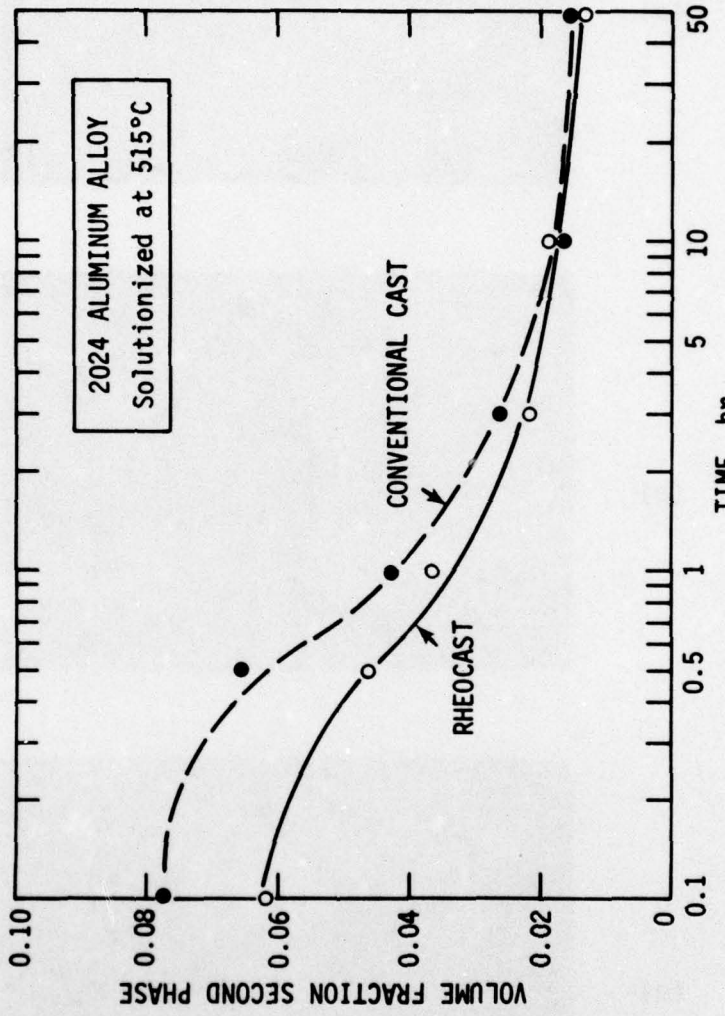

Figure 15. Plot of experimentally measured volume fraction of second phase as a function of solution time at 515°C for conventional cast and Rheocast 2024 aluminum base alloy.

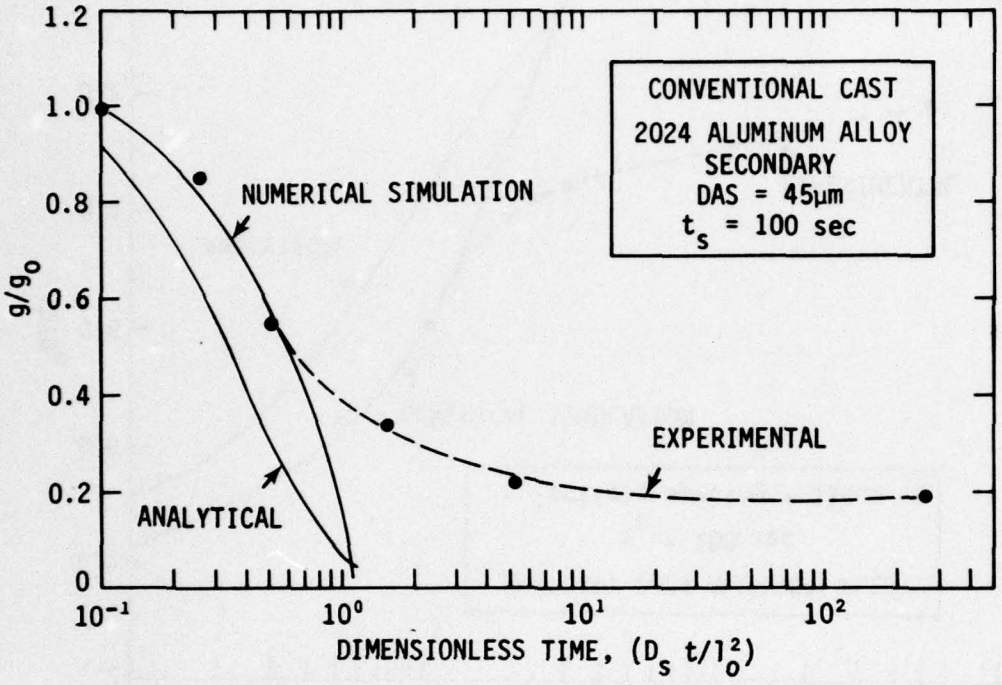

Figure 16. Plot of normalized second phase content, g/g_0, as a function of dimensionless time, $D_s t/l_0^2$ for a conventionally cast 2024 aluminum base alloy. The plots were determined by analytical and numerical solution of the solutionization model employing a plate-like dendrite morphology.

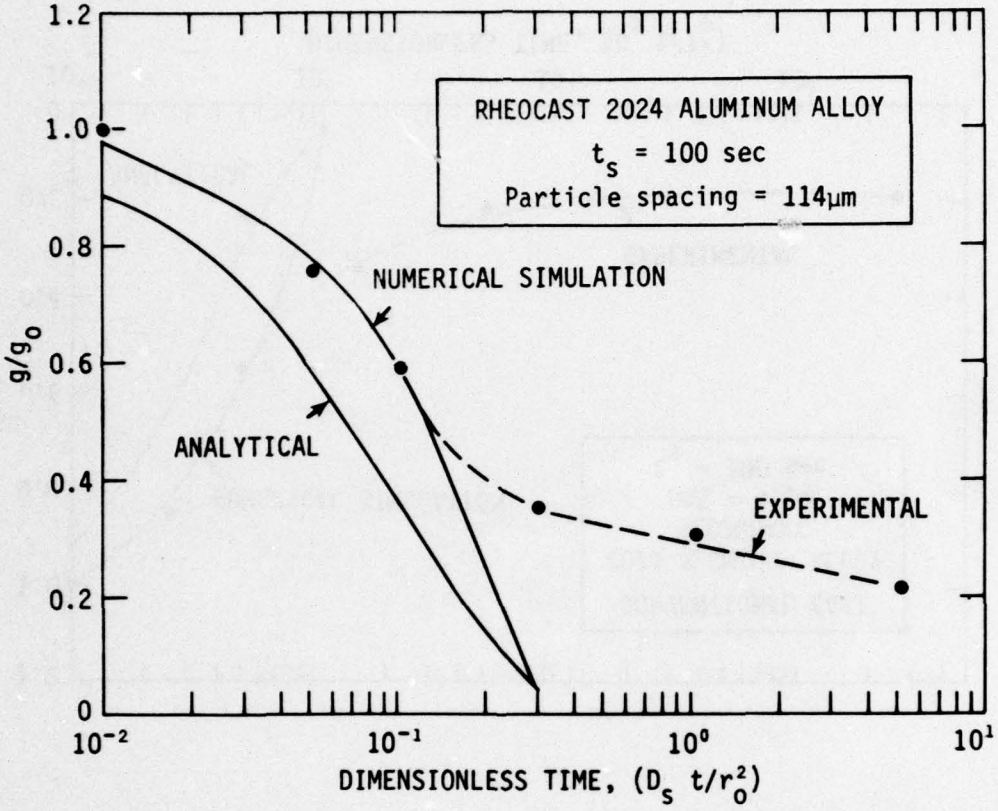

Figure 17. Plot of normalized second phase content, g/g_0; as a function of dimensionless time, $D_s t/l_0^2$, for a Rheocast 2024 aluminum base alloy. The plots were determined by analytical and numerical solution of the solutionization model employing a spherical growth morphology.

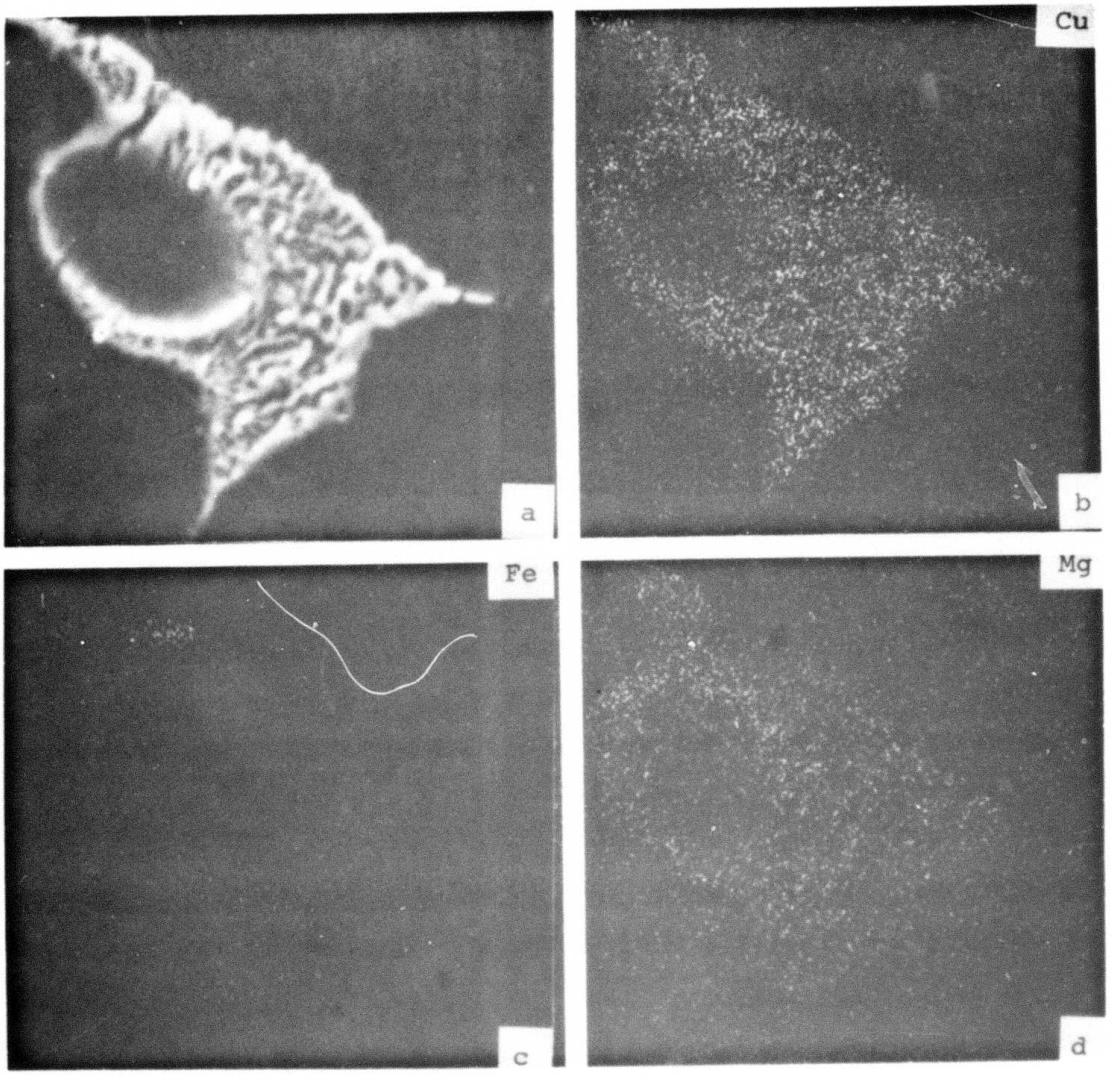

Figure 18. Secondary Electron Image and elemental x-ray maps of a second phase particle in the conventional cast 2024 aluminum base alloy prior to heat treatment. (a) SEI; (b), (c), and (d) are x-ray elemental maps of copper, iron, and magnesium, respectively; magnification: 1000X.

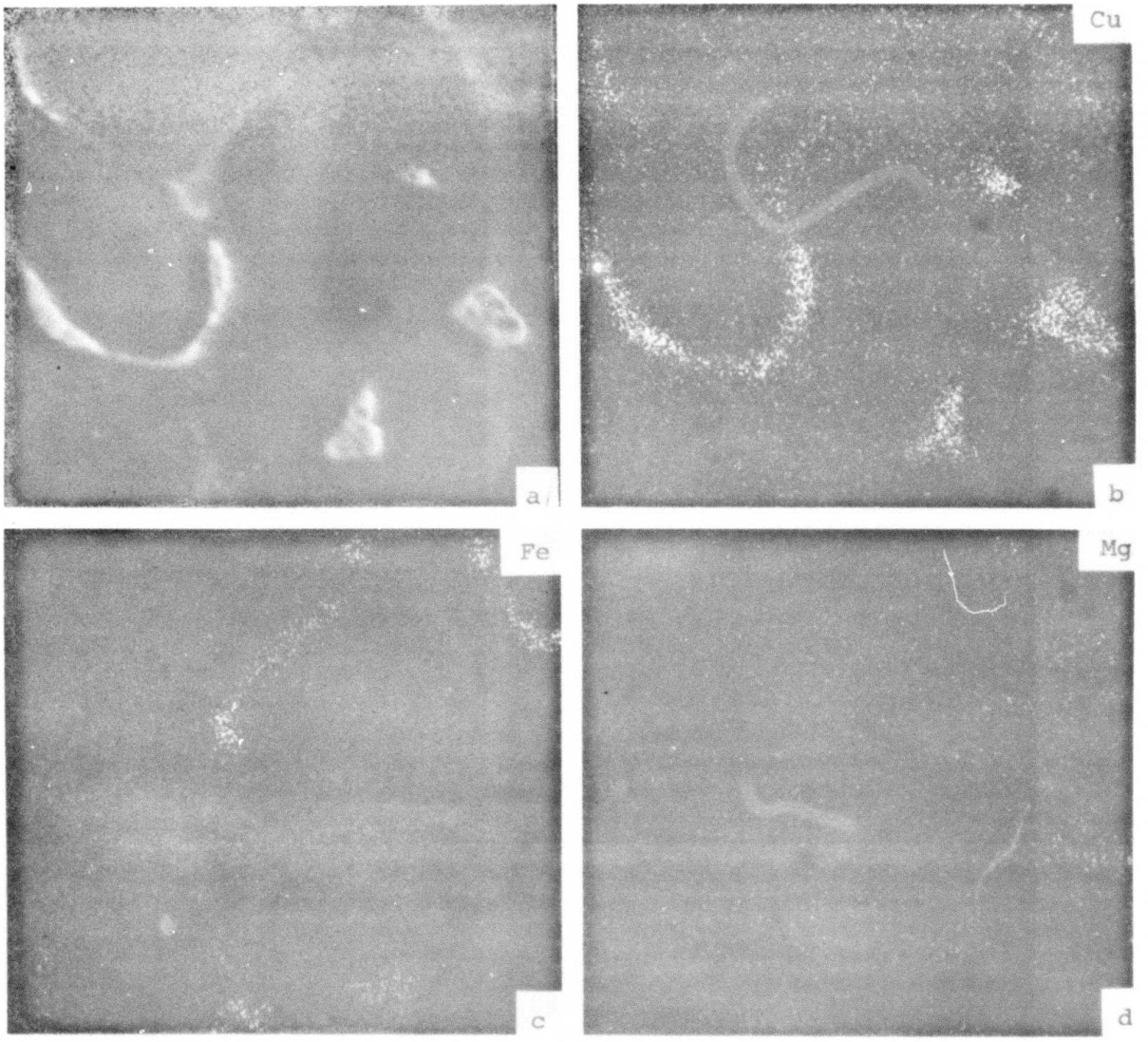

Figure 19. Secondary Electron Image and elemental x-ray maps of second phase particles in the Rheocast 2024 aluminum base alloy prior to heat treatment. (a) SEI; (b), (c), and (d) are x-ray elemental maps of copper, iron, and magnesium, respectively; magnification: 1000X.

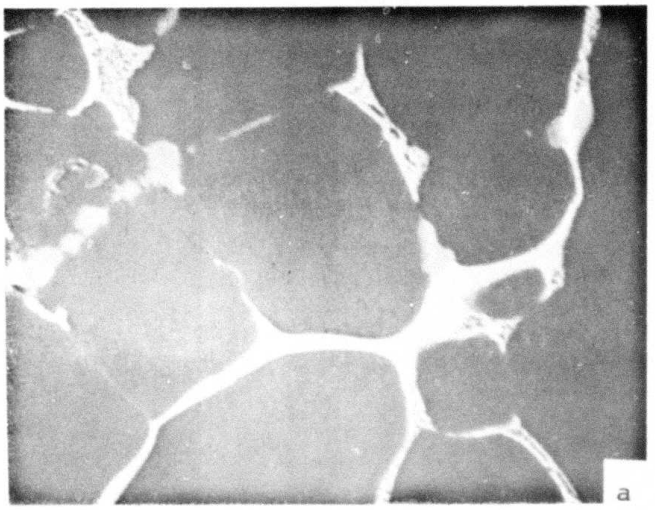

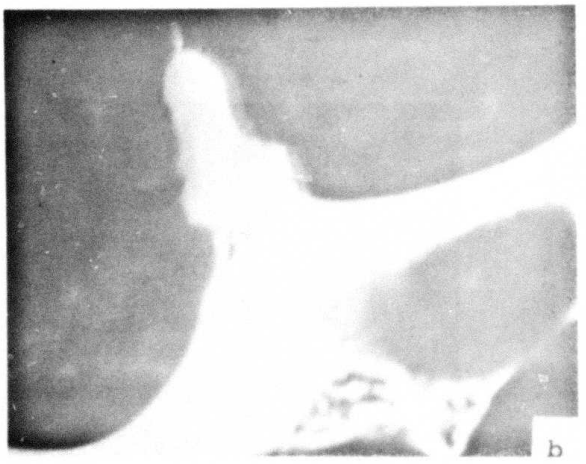

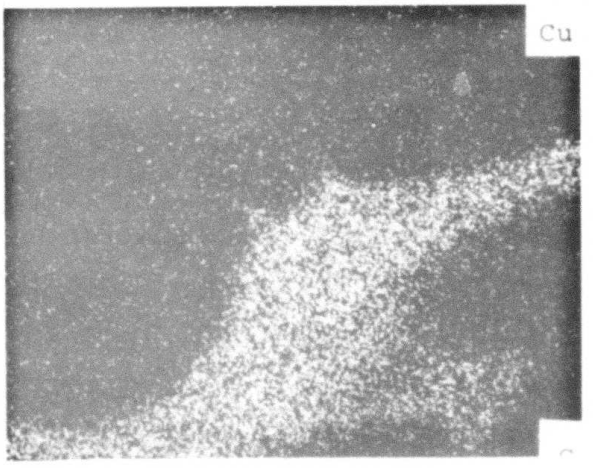

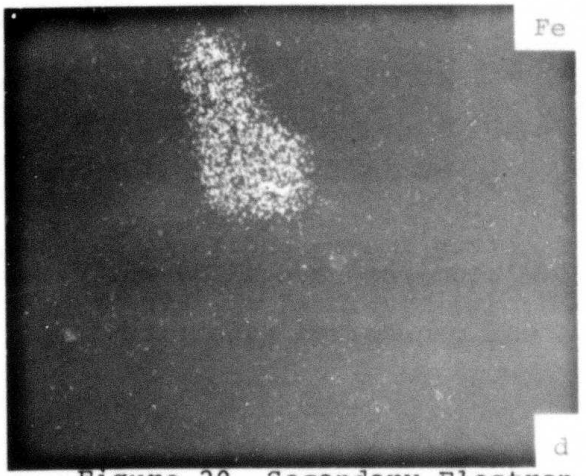

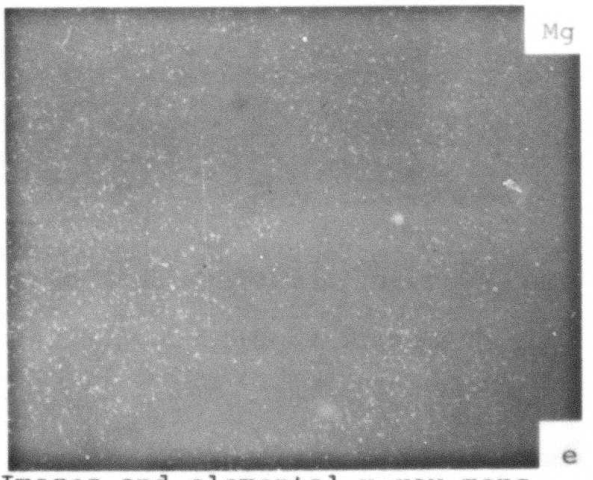

Figure 20. Secondary Electron Images and elemental x-ray maps of second phase particles in Rheocast 2024 aluminum base alloy after a heat treatment of 1/2 hr. (a) and (b) are SEI's at 300X and 1000X magnification, respectively. (c), (d), and (e) are x-ray elemental maps of copper, iron, and magnesium, respectively, at 1000X magnification.

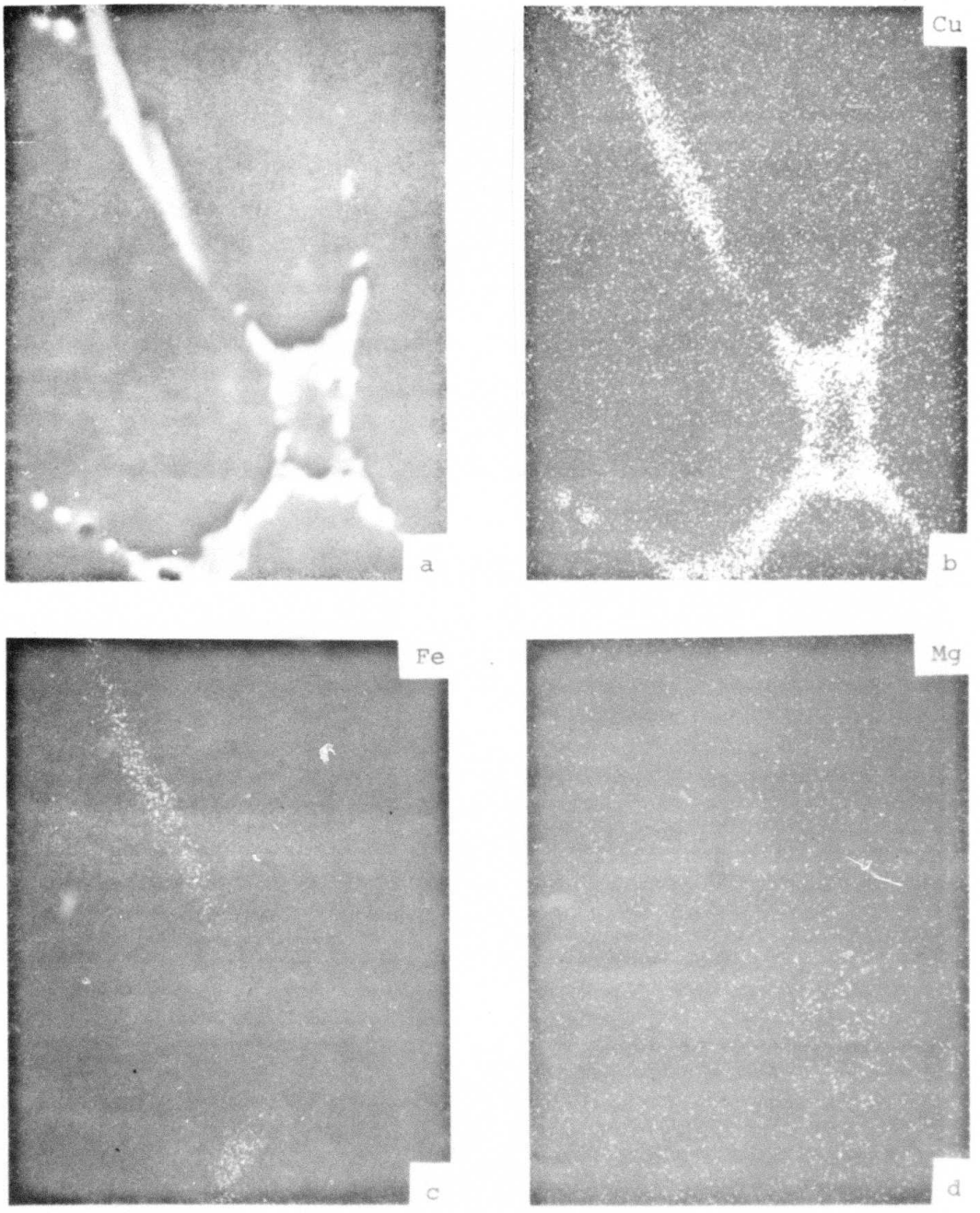

Figure 21. Secondary Electron Images and x-ray elemental maps of conventional cast 2024 aluminum base alloy after a heat treatment of 10 hrs. (a) SEI; (b), (c), and (d) are x-ray elemental maps of copper, iron, and magnesium; magnification: 1000X.

DISTRIBUTION LIST

No. of Copies	To
1	Office of the Director, Defense Research and Engineering, The Pentagon, Washington, D. C. 20301
12	Commander, Defense Documentation Center, Cameron Station, Building 5, 5010 Duke Street, Alexandria, Virginia 22314
1	Metals and Ceramics Information Center, Battelle Columbus Laboratories, 505 King Avenue, Columbus, Ohio 43201
	Deputy Chief of Staff, Research, Development, and Acquisition, Department of the Army, Washington, D. C. 20310
1	ATTN: DAMA-ARZ
	Commander, Army Research Office, P. O. Box 12211, Research Triangle Park, North Carolina 27709
1	ATTN: Information Processing Office
	Commander, U. S. Army Materiel Development and Readiness Command, 5001 Eisenhower Avenue, Alexandria, Virginia 22333
1	ATTN: DRCLDC, Mr. R. Zentner
	Commander, U. S. Army Electronics Research and Development Command, Fort Monmouth, New Jersey 07703
1	ATTN: DRSEL-GG-DD
1	DRSEL-GG-DM
	Commander, U. S. Army Missile Research and Development Command, Redstone Arsenal, Alabama 35809
1	ATTN: Technical Library
	Commander, U. S. Army Armament Research and Development Command, Dover, New Jersey 07801
2	ATTN: Technical Library
1	DRDAR-SCM, J. D. Corrie
	Commander, U. S. Army Satellite Communications Agency, Fort Monmouth, New Jersey 07703
1	ATTN: Technical Document Center
	Commander, U. S. Army Tank-Automotive Research and Development Command, Warren, Michigan 48090
2	ATTN: DRDTA-UL, Technical Library
	Commander, White Sands Missile Range, New Mexico 88002
1	ATTN: STEWS-WS-VT

No. of Copies	To
	Commander, Aberdeen Proving Ground, Maryland 21005
1	ATTN: STEAP-TL, Bldg. 305
	Commander, Frankford Arsenal, Philadelphia, Pennsylvania 19137
1	ATTN: Library, H1300, Bl. 51-2
	Commander, Picatinny Arsenal, Dover, New Jersey 07801
1	ATTN: SARPA-RT-S
	Commander, Redstone Scientific Information Center, U. S. Army Missile Command, Redstone Arsenal, Alabama 35809
4	ATTN: DRDMI-TB
	Chief, Benet Weapons Laboratory, LCWSL, USA ARRADCOM, Watervliet, New York 12189
1	ATTN: DRDAR-LCB-TL
	Commander, U. S. Army Foreign Science and Technology Center, 220 7th Street, N. E., Charlottesville, Virginia 22901
1	ATTN: Military Tech, Mr. Marley
	Director, Eustis Directorate, U. S. Army Air Mobility Research and Development Laboratory, Fort Eustis, Virginia 23604
1	ATTN: Mr. J. Robinson, DAVDL-E-MOS (AVRADCOM)
	U. S. Army Aviation Training Library, Fort Rucker, Alabama 36360
1	ATTN: Building 5906-5907
	Naval Research Laboratory, Washington, D. C. 20375
1	ATTN: Dr. J. M. Krafft - Code 8430
	Chief of Naval Research, Arlington, Virginia 22217
1	ATTN: Code 471
	Air Force Materials Laboratory, Wright-Patterson Air Force Base, Ohio 45433
2	ATTN: AFML/MXE/E. Morrissey
1	AFML/LC
1	AFML/LLP/D. M. Forney, Jr.
1	AFML/MBC/Mr. Stanley Schulman
	National Aeronautics and Space Administration, Washington, D. C. 20546
1	ATTN: Mr. B. G. Achhammer
1	Mr. G. C. Deutsch - Code RW
	National Aeronautics and Space Administration, Marshall Space Flight Center, Huntsville, Alabama 35812
1	ATTN: R. J. Schwinghammer, EH01, Dir, M&P Lab
1	Mr. W. A. Wilson, EH41, Bldg. 4612

No. of Copies	To
1	Ship Research Committee, Maritime Transportation Research Board, National Research Council, 2101 Constitution Ave., N. W., Washington, D. C. 20418
2	Director, Defense Advanced Research Projects Agency, 1400 Wilson Boulevard, Arlington, Virginia 22209
	Wyman-Gordon Company, Worcester, Massachusetts 01601
1	ATTN: Technical Library
	TRW Incorporated, 23555 Evelid Avenue, Cleveland, Ohio 44117
1	ATTN: William Spiegelberg, Code T-M 2365
	Norris Laboratory, 10526 Gateridge Road, Cockeysville, Maryland 21030
1	ATTN: Mr. Victor Norris
	Director, Army Materials and Mechanics Research Center, Watertown, Massachusetts 02172
2	ATTN: DRXMR-PL
1	DRXMR-AP
1	DRXMR-X
1	DRXMR-XP
1	DRXMR-CT
1	DRXMR-ER, Mr. F. C. Quigley
1	DRXMR-E

Army Materials and Mechanics Research Center
Watertown, Massachusetts 02172
MACHINE CASTING OF FERROUS ALLOYS
R. Mehrabian, D.G. Backman, G.J. Abbaschian
C.Y. Chen, S. Hong, S.D.E. Ramati and Y.V. Murty

AD______________
UNCLASSIFIED
UNLIMITED DISTRIBUTION

Technical Report AMMRC TR 78-23, May 1978
68 pp - illustrations, tables, DAAG46-76-C-0023
D/A Project ARPA Order No. 2267 AMCMS Code
6Y10, Final Report October 1, 1975 to December 31, 1977

Key Words
Die Casting
Solidification
Ferrous Alloys

This is the fourth and final report describing research conducted at the University of Illinois at Urbana-Champaign as part of a joint University-Industry research program on machine casting of high temperature alloys. It covers the period of 30 months, 1 October 1975 to 31 December 1977. This final report summarizes earlier results reported in the first eighteen months of the program and covers the details of the investigation in the last twelve months. These include the following: (1) A description of the castings systems developed in this study and a summary of all the findings on the relationship between process variables and Rheocast structures, (2) A summary of the relationships developed between gating systems, process variables and mold filling characteristics of different viscosity materials and low temperature alloy slurries, (3) the effect of cast (Rheocast) structure on microsegregation, solution heat treatment response, and mechanical properties of high temperature alloys, (4) Analytical and computer models developed for solutionizing of Rheocast and conventional cast alloys. Comparison between predictions of the model and experimental findings on aluminum alloy 2024, and (5) A summary of cost analysis model developed and prediction of cost per piece for a previously investment cast part.

Army Materials and Mechanics Research Center
Watertown, Massachusetts 02172
MACHINE CASTING OF FERROUS ALLOYS
R. Mehrabian, D.G. Backman, G.J. Abbaschian
C.Y. Chen, S. Hong, S.D.E. Ramati and Y.V. Murty

AD______________
UNCLASSIFIED
UNLIMITED DISTRIBUTION

Technical Report AMMRC TR 78-23, May 1978
68 pp - illustrations, tables, DAAG46-76-C-0023
D/A Project ARPA Order No. 2267 AMCMS Code
6Y10, Final Report October 1, 1975 to December 31, 1977

Key Words
Die Casting
Solidification
Ferrous Alloys

This is the fourth and final report describing research conducted at the University of Illinois at Urbana-Champaign as part of a joint University-Industry research program on machine casting of high temperature alloys. It covers the period of 30 months, 1 October 1975 to 31 December 1977. This final report summarizes earlier results reported in the first eighteen months of the program and covers the details of the investigation in the last twelve months. These include the following: (1) A description of the castings systems developed in this study and a summary of all the findings on the relationship between process variables and Rheocast structures, (2) A summary of the relationships developed between gating systems, process variables and mold filling characteristics of different viscosity materials and low temperature alloy slurries, (3) the effect of cast (Rheocast) structure on microsegregation, solution heat treatment response, and mechanical properties of high temperature alloys, (4) Analytical and computer models developed for solutionizing of Rheocast and conventional cast alloys. Comparison between predictions of the model and experimental findings on aluminum alloy 2024, and (5) A summary of cost analysis model developed and prediction of cost per piece for a previously investment cast part.

Army Materials and Mechanics Research Center
Watertown, Massachusetts 02172
MACHINE CASTING OF FERROUS ALLOYS
R. Mehrabian, D.G. Backman, G.J. Abbaschian
C.Y. Chen, S. Hong, S.D.E. Ramati and Y.V. Murty

AD______________
UNCLASSIFIED
UNLIMITED DISTRIBUTION

Technical Report AMMRC TR 78-23, May 1978
68 pp - illustrations, tables, DAAG46-76-C-0023
D/A Project ARPA Order No. 2267 AMCMS Code
6Y10, Final Report October 1, 1975 to December 31, 1977

Key Words
Die Casting
Solidification
Ferrous Alloys

This is the fourth and final report describing research conducted at the University of Illinois at Urbana-Champaign as part of a joint University-Industry research program on machine casting of high temperature alloys. It covers the period of 30 months, 1 October 1975 to 31 December 1977. This final report summarizes earlier results reported in the first eighteen months of the program and covers the details of the investigation in the last twelve months. These include the following: (1) A description of the castings systems developed in this study and a summary of all the findings on the relationship between process variables and Rheocast structures, (2) A summary of the relationships developed between gating systems, process variables and mold filling characteristics of different viscosity materials and low temperature alloy slurries, (3) the effect of cast (Rheocast) structure on microsegregation, solution heat treatment response, and mechanical properties of high temperature alloys, (4) Analytical and computer models developed for solutionizing of Rheocast and conventional cast alloys. Comparison between predictions of the model and experimental findings on aluminum alloy 2024, and (5) A summary of cost analysis model developed and prediction of cost per piece for a previously investment cast part.

Army Materials and Mechanics Research Center
Watertown, Massachusetts 02172
MACHINE CASTING OF FERROUS ALLOYS
R. Mehrabian, D.G. Backman, G.J. Abbaschian
C.Y. Chen, S. Hong, S.D.E. Ramati and Y.V. Murty

AD______________
UNCLASSIFIED
UNLIMITED DISTRIBUTION

Technical Report AMMRC TR 78-23, May 1978
68 pp - illustrations, tables, DAAG46-76-C-0023
D/A Project ARPA Order No. 2267 AMCMS Code
6Y10, Final Report October 1, 1975 to December 31, 1977

Key Words
Die Casting
Solidification
Ferrous Alloys

This is the fourth and final report describing research conducted at the University of Illinois at Urbana-Champaign as part of a joint University-Industry research program on machine casting of high temperature alloys. It covers the period of 30 months, 1 October 1975 to 31 December 1977. This final report summarizes earlier results reported in the first eighteen months of the program and covers the details of the investigation in the last twelve months. These include the following: (1) A description of the castings systems developed in this study and a summary of all the findings on the relationship between process variables and Rheocast structures, (2) A summary of the relationships developed between gating systems, process variables and mold filling characteristics of different viscosity materials and low temperature alloy slurries, (3) the effect of cast (Rheocast) structure on microsegregation, solution heat treatment response, and mechanical properties of high temperature alloys, (4) Analytical and computer models developed for solutionizing of Rheocast and conventional cast alloys. Comparison between predictions of the model and experimental findings on aluminum alloy 2024, and (5) A summary of cost analysis model developed and prediction of cost per piece for a previously investment cast part.